Renewable and Sustainable Energy Reviews 200 (2024) 114579

Contents lists available at ScienceDirect

Renewable and Sustainable Energy Reviews

journal homepage: www.elsevier.com/locate/rser

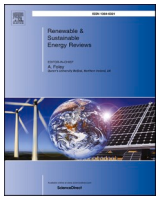

Contemporary advances in organic thermoelectric materials: Fundamentals, properties, optimization strategies, and applications

Misbah Sehar Abbasi [a], Rabia Sultana [b], Iftikhar Ahmed [c], Muhammad Adnan [d,e], Usman Ali Shah [f], Muhammad Sultan Irshad [g,**], Hung Ngoc Vu [h], Lien Thi Do [h], Hong Ha Thi Vu [h], Thuy-Duong Pham [h], Ho Xuan Nang [i], Van-Duong Dao [h,*]

[a] College of Materials Science and Optoelectronic Technology, University of Chinese Academy of Sciences, Beijing, 100049, PR China
[b] College of Resources and Environment, University of Chinese Academy of Sciences, Beijing, 100049, PR China
[c] Environmental and Public Health Department, College of Health Sciences, Abu Dhabi University, P.O. Box 59911, Abu Dhabi, United Arab Emirates
[d] Engineering Laboratory of Advance Energy Materials, Ningbo Institute of Materials Technology and Engineering, Chinese Academy of Sciences, Ningbo, 315201, PR China
[e] Physics Department, GC University Hyderabad, Sindh Pakistan, Pakistan
[f] Department of Physics and Astronomy, University of Florence, Via Giovanni Sansone, 1, Sesto Fiorentino, I-50019, Florence, Italy
[g] School of Materials Science and Engineering, Hubei University, Wuhan, 430062, PR China
[h] Faculty of Biotechnology, Chemistry, and Environmental Engineering, PHENIKAA University, Hanoi, 100000, Viet Nam
[i] Faculty of Vehicle and Energy Engineering, PHENIKAA University, Hanoi, Viet Nam

ARTICLE INFO

Keywords:
Organic
Thermoelectric
Materials
Mechanisms
Challenges

ABSTRACT

Thermoelectric material's capacity to directly transform waste heat into useable energy has captured the interest of delving into the complexities of sustainable development. Indeed, organic thermoelectric (OTE) materials are gaining momentum for wearable and portable electronics owing to low density, high flexibility, and eco-friendliness. Herin, this review is designed to boost the interest of researchers in the fundamentals of TE, recent significant progress, and fabrication techniques of polymer-based TE materials. Firstly, recent advancements in synthesizing novel materials and understanding doping methods to enhance conductivity are overviewed. The focus then shifts towards emphasizing the novel and distinctive approach of integrating carbon nanotubes, graphene, and ternary composites with OTEs. Finally, a few applications are demonstrated, the challenges encountered in creating the subsequent origination of polymer-based materials with outstanding TE performance are explored, and further insights are discussed.

1. Introduction

With ever-depleting energy resources and rising sustainability issues, the need for innovation to generate electricity is becoming more imperative [1,2]. Global trends are shifting greatly towards exploring ways to create renewable energy and thermoelectric (TE) materials have been justified as an apt solution to this ever-growing field due to the direct conversion of heat into electricity [3]. The progress of wearable electronic and implantable medical devices, for instance, wearable pressure sensors [4], pulse-oximetry sensors [5], electrocardiography monitoring sensors [6], biometric monitors [7], along with implantable cardiac pacemakers [8], neurological and sensory devices [9], etc. is drastically growing in biomedical engineering. Along with the inherent conversion ability of TEs, the significance of these materials is greatly enhanced owing to their small size, static parts, and high conversion efficiency, leading to obsoleting the conventional power generation methods over the years. The exploration of TE materials possessing high efficiency has been greatly emphasized. Figure of merit, i.e. [10].

$$zT = \frac{S^2\sigma}{\kappa}T = \frac{S^2\sigma}{\kappa_e + \kappa_l}T \quad (1)$$

is a measure of the efficiency of TE materials for energy conversion where S represents the Seebeck coefficient measured in VK^{-1}, σ depicts electrical conductivity in Sm^{-1}, T is absolute temperature measured in kelvins K, whereas κ shows thermal conductivity composed up of both

* Corresponding author.
** Corresponding author.
E-mail addresses: muhammadsultanirshad@hubu.edu.cn (M.S. Irshad), duong.daovan@phenikaa-uni.edu.vn (V.-D. Dao).

https://doi.org/10.1016/j.rser.2024.114579
Received 27 October 2023; Received in revised form 10 May 2024; Accepted 15 May 2024
Available online 29 May 2024

List of abbreviations

CNT	Carbon Nanotube
COFs	Covalent Organic Frameworks
DC	Direct Current
DWCNT	Double-Walled Carbon Nanotubes
E_{dif}	Energy Difference
GO	Graphite Oxide
HOMO	Highest Occupied Molecular Orbital
K	Kelvin
LBL	Layer-By-Layer
LUMO	Lowest Unoccupied Molecular Orbital
MWCNT	Multi-Walled Carbon Nanotubes
n	Carrier Concentration
NDI	Naphthalene Diimide
OSCs	Organic Semiconductors
OTE	Organic Thermoelectric
OTEG	Organic Thermoelectric Generators
OTFTs	Organic Thin-Film Transistors
PANI	Polyaniline
PF	Power Factor
S	Seebeck Coefficient
SWCNT	Single-Walled Carbon Nanotubes
T	Absolute Temperature
TE	Thermoelectric
TED	Thermo Electric Devices
TEG	Thermo Electric Generators
TEM	Thermo Electric Module
zT	Figure of merit
κ	Thermal Conductivity
κ_e	electronic thermal conductivity
κ_l	lattice thermal conductivity
μ	Charge Carrier
σ	Electrical Conductivity

the carrier thermal conductivity (κ_e) and lattice thermal conductivity (κ_l) measured in $Wm^{-1}K^{-1}$ and $S^2\sigma$ is commonly described as the power factor (*PF*).

Significant attempts were made to boost the figure-of-merit (zT) of TE generators (TEG) by using inorganic semiconductors as active components along with high-performance TE materials [11]. Indeed, inorganic TE materials (e.g., Te, Bi, Pb) are confined in resource, hazardous, and synthesized using high-temperature techniques that are inconsistent with mass production, limiting broad-range applications of TE materials [12]. Organic semiconductor (OSC) materials, in contrast, are carbon-based, economical, and solution-processed. Furthermore, the mechanical flexibility of OSC allows such devices to be used in applications, including wearable electronics, sensors, and domotics [13,14]. The operating temperature range of inorganic and organic TE generators (OTEGs) differ significantly; while organic TEGs typically operate at temperatures under 450 K, which equates to the majority of the world's waste heat, the operating temperature range of inorganic TEGs is reasonably high (often 600 K) [15–17]. As a result, organic TEGs regenerate waste heat at temperatures closer to T_{amb} while delivering efficient electricity production for use in wearable, biomedical, and domotic applications [18].

Synthesis of new materials and new doping strategies can enhance the commercial scope of OTEGs [19]. Since the TE voltage produced by one TEG is often insignificant, TE couplings of p-type and n-type elements (described as legs) must be series-coupled to provide sufficient power for well-designed operations. TEGs are an appealing answer to energy and environmental challenges since they may be employed in cooling and power production applications without shifting components or harmful operational fluids. While there is experimental confirmation zT of ~0.4 for OSC, it encounters low electrical conductivity; hence, novel materials, doping methods, or relevant processes need to be developed to improve the figure of merit [20–23], in OTEGs. Additionally, graphene and carbon nanotubes combined with OTEs are effective for TE performance optimization after being used as a prospective TE material [24]. They are incorporated as filler or a composite second phase in conductive polymers [25].

Herein, this review aims to overview contemporary advances in organic thermoelectric materials and their potential applications. Firstly, it delves into the core principles underlying thermoelectric (TE) materials, elucidating their fundamental properties and behaviors. Furthermore, it aims to showcase the integration of diverse organic-based TE materials, exploring their synthesis methodologies, distinctive properties, and the innovative fabrication techniques employed in their fabrication. Notably, it explores the groundbreaking fusion of contemporary nanomaterials like carbon nanotubes, graphene, and ternary composites with polymers, marking a significant milestone in recent investigations endeavors aimed at enhancing the figure of merit. Lastly, it sheds light on the emerging commercial applications of TE materials, highlighting their potential transformative impact in fields such as home automation (domotics) and lifestyle enhancement. Through this comprehensive exploration, this review seeks to provide a holistic understanding of TE materials, from their theoretical underpinnings to their practical applications, thereby contributing to the advancement of this emerging field.

2. Fundamentals of TE materials

2.1. Working modes

On operational grounds, TE materials are categorized into three modes, which include the Seebeck effect, Thomson effect, and Peltier effect which are discussed in the subsections [26].

2.1.1. Seebeck effect

Owing to their ability to harvest heat from the waste, these materials were first discovered in 1821 by Thomas Johann, and are capable of performing waste heat energy conversion directly into electricity by forming a temperature gradient that permits the diffusion of n-type electrons from the hotter end to the cooler one and the other way round for p-type holes which are termed as Seebeck effect [27]. At one end, the accumulation of charge carriers is a result of this diffusion, as demonstrated in (Fig. 1I (a)). The voltage that results from this charge accumulation is closely correlated with the temperature difference across the semiconductor. TEG semiconductor devices generate electricity using the Seebeck effect. Electrical current is driven by the voltage that is produced, and this current, in turn, produces useable power at a load. Typically, the Seebeck effect (S) can be expressed mathematically as

$$S = -\frac{\nabla V}{\nabla T} \tag{2}$$

V represents the voltage gradient between two ends of the material, S is the Seebeck coefficient (V/K), and T represents the temperature gradient (K). This effect is commonly used in thermocouples. These generators are reliable, quiet, independent of fuels and greenhouse gases to function, can be operated in any direction, and perform well under high-G or zero-G conditions. They are scalable to generate output greater than kilowatts and less than microwatts. They are compact and perform direct conversion.

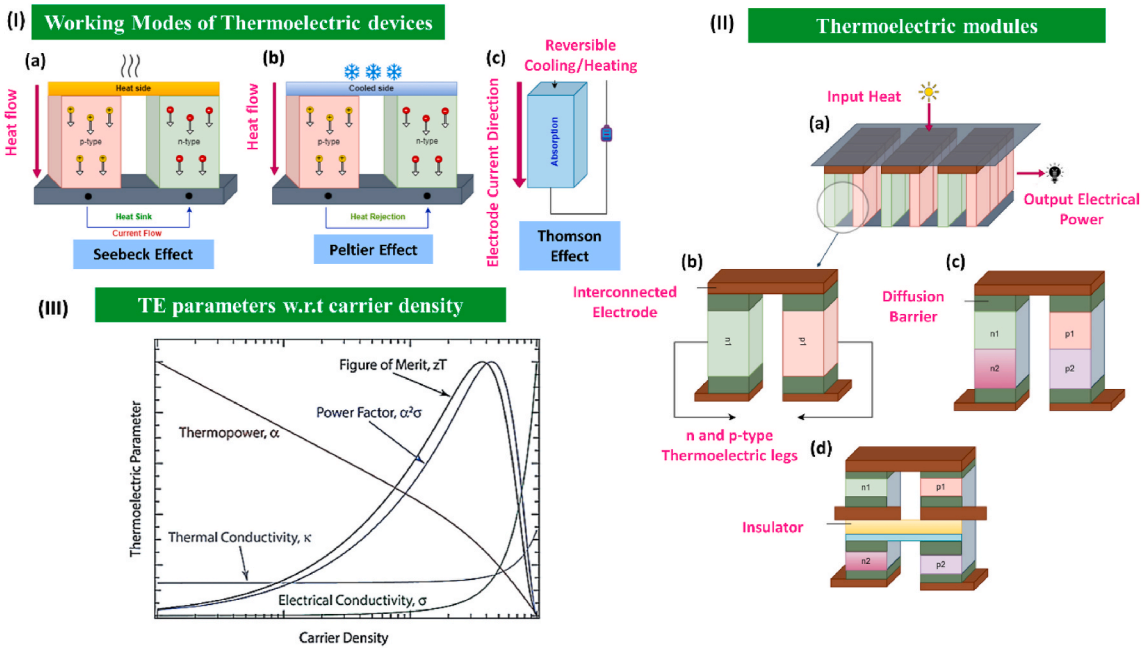

Fig. 1. (I) Working Modes of TE Devices (a) Seebeck Effect (b) Peltier Effect (c) Thomson Effect (II) (a) TE module comprises of p and n-types TE legs (b) single thermocouple (c) segmented thermocouple (d) cascade thermocouple (III). Featuring the dependence of TE parameters w.r.t carrier density for carbon nanotubes [38]. Copyright 2018, Wiley-VCH.

2.1.2. Peltier effect

The peltier effect has the advantage of forcing a temperature gradient with an external electric current. A voltage is applied across linked conductors to produce an electric current. As current flows through the intersections of two conductors, cooling occurs at one terminal as heat is dissipated, as seen in (Fig. 1I (b)). Heat is transferred to the opposite joint. Most frequently, cooling is accomplished using the Peltier effect. The Peltier effect controls how TE coolers (TECs) work. The temperature can be increased or decreased using the Peltier effect. In all circumstances, a DC voltage is required [28]. TE coolers are a great alternative when conventional cooling techniques fail. Also, compared to other cooling equipment on the market, TE coolers are more environmentally friendly. No chlorofluorocarbons or refrigerant emissions, a long lifespan, performance independent of orientation, compatibility with severe environments or far-off locations, controllability, the ability to cool well under ambient temperatures, and low maintenance are some benefits of using TE cooling in electronic devices [29]. Moreover, coolers can greatly enhance the following characteristics of client electronic systems: thermal performance, noise, weight, cost, efficiency, and size. The cooling productivity of a cooling device is defined by the coefficient of performance (*COP*), which is given in Equation (3).

$$COP_{max} = \left(\frac{T_{cold}}{T_{hot} - T_{cold}}\right)\left(\frac{\sqrt{1+ZT} - \frac{T_{hot}}{T_{cold}}}{\sqrt{1+ZT}+1}\right) \tag{3}$$

The hot-side and cold-side temperatures are T_{hot} and T_{cold}, respectively. A greater zT value is preferable for cooling and power-generating applications. Higher zT values suggest improved material performance, resulting in an increased COP_{max}. The Peltier effect generates heat absorption and dissipation, which affects the cooler's efficiency.

2.1.3. Thomson effect

Whenever a single conductor is subjected to an electric current, the Thomson effect is generated inside it due to temperature gradient as shown in (Fig. 1 (I)(c)). Heat conducted (Q) this way is directly proportional to the temperature gradient and current intensity as follows:

$$\mathscr{Q} = \mu \bullet I \bullet \nabla T \tag{4}$$

whereas I represents the current intensity (A), V/K stands for the Thomson coefficient, and T stands for the temperature differential (K). When heat is evolved, a positive Thomson effect is produced. However, it is negative when heat is absorbed [30].

2.2. Designing TE device

Fossil fuels are used to meet the world's energy needs, leading to greenhouse gas emissions and climate change. Similarly, a large quantity of energy is being wasted in various exhaust forms such as automobile exhaust, heated combustion gases spilled into the atmosphere, and hot fluids discharged into the surroundings. In power production mode, TE devices (TED) employ the Seebeck effect. Peltier effect is operated in thermal management mode. The versatility of TEDs makes them appealing for niche functions, including accurate temperature control. A TED is comprised of many n-type and p-type semiconductor material thermocouples, which are electrically and thermally linked in series [31]. To prevent heat from diffusing to the cold side, a TE module (TEM) is built with heat sinks on both the hot and bleak surfaces, as well as additional interface and insulating layers. (Fig. 1 (II)(a)) depicts the schematic of the TE module with p-type and n-type TE legs. The thermocouples are alternatively linked in electrical series but in a thermally parallel connection by interconnecting electrodes (Figure (II)(b)) to properly feed thermal power to the legs and efficiently extract electric power from the legs, the link between the metallic electrodes must have very short electrical contact resistance. Stacking several components or legs (segment type) or stacking various modules (cascade type) are efficient ways to increase conversion efficiency [32]. By stacking materials or legs with a high zT at a high temperature on top of materials or legs with a high zT at a low temperature, a segmented thermocouple module is created (Fig. 1 (II)(c)). At least two separate modules are employed in a cascaded thermocouple module. A module that performs well at an increased temperature is layered on top of another module that performs well at a lower temperature (Fig. 1 (II)(d)).

[33]

Current TEG modeling research has considerably improved its speed and accuracy. Benefits of improved modeling and simulation save money by lowering the cost of a product or project over its lifespan; continuous prototype iterations and testing are costly, and it is better to solve problems now rather than later, at a much higher cost and with less time, and to examine complex systems.

2.3. Parameters for efficiency of TE material

A high *PF* value suggests large current and voltage outputs from the device. A highly efficient TE material must undergo a high zT value, which means *PF* and temperature should be elevated while keeping the thermal conductivity minimum [33]. Along with the requirements of higher zT value and lower cost, a good TE material must also possess adequate mechanical strength and higher thermal stability for robust fabrication and long-term device services, respectively [34]. However, the three quantities S, σ, and κ are not independent of each other; instead, they are strongly positively correlated, and therefore it is practically impossible to singularly vary any one of them whilst keeping the others constant [35]. Fig. 1 (III) demonstrates the dependence of TE parameters w.r.t carrier density for carbon nanotubes. Their dependence causes a strong hindrance to the enhancement of the zT values of TE materials. Nonetheless, an adjustment can be made between the three quantities to output the maximum zT value. Therefore, enhancement of the zT value of a TE material by optimizing any of these properties tends to be a very challenging task as the increment of one property may result in a significant decrement of the other. For example, the improvement of the Seebeck coefficient (S) causes a decreased electrical conductivity (σ) value, while the Wiedemann-Franz law shows that the κ_t and σ have a direct relationship in between [36]. Thus, the requirement is to find a way to optimize all the properties simultaneously to get a high zT value. zT improvement stems either from the increase of *PF* or from the decrease of lattice thermal conductivity (κ_{lat}), carried out via microstructure engineering techniques.

Since *PF* depends on S, various techniques have been reported to increase the Seebeck coefficient, including the energy filtering effect, band engineering, tuning of effective masses for density of states (DOS), and optimized doping levels. The energy filtering effect impedes low energy carriers, which practically increases S leading to an improved zT value [37]. Furthermore, band engineering also improves S by altering or controlling the bandgap. Both the reduced energy difference (E_{dif}) between valence bands and the enlarged band gap contribute greatly to the increase Seebeck effect.

Additionally, both the charge carrier (μ) and the carrier concentration (n) are directly proportional to σ; therefore, both n and μ of a TE material must be kept as high as possible to increase its σ value. External doping of p-type or n-type impurities effectively increases electrical conductivity, but the impurity scattering effect reduces the carrier mobility. However, high mobility can be achieved using a modulation doping technique that isolates the carrier from the matrix material pace. Phonon-phonon scattering, caused by lattice thermal conduction phonons, is another phenomenon that affects κ and, thereby, the zT value. Nanostructuring hampers phonon transport and thus deters thermal conductivity, which consequently improves the zT value. Photon scattering and low dimensionality are considered to be the active means of diminishing the material's thermal conductivity.

2.4. Modeling and optimization of TE materials

A recent report by Firth et al. [39] on life cycle study shows that in 2030, nearly half of the global energy may finish as waste heat. TEGs with n-type and p-type components under insulating ceramic substrates have been applied in the industry. Simulation and modeling are two tools that can be employed to validate the design of a TEG [40]. Ranjan et al. used the finite element method (FEM) to study a 3D model of TEG with 196 legs for different energy losses [41]. The result revealed that in an isothermal state, the maximum power output can be obtained for cylindrical legs provided a hot end temperature kept at 800 K. Whereas, further findings on Taguchi and ANOVA methods showed a power output of 48 W and a maximum efficiency of 12.8 % has been predicted. Optimum length of leg area of 4 mm^2 and length of 2 mm at 6 Ω load resistance have been estimated as combinations for maximizing power output.

2.5. Role of nanoparticles in TE efficiency

The TE effect makes it possible to transform leftover heat into electrical power. Commercial wristwatches are already available which use TE power and make use of the temperature variance between the body and surroundings. Higher solar-to-electricity conversion efficiencies can be achieved by combining PV with TE effects. The TE effect may convert the remaining solar energy from the range of 800 nm up to approximately 2500 nm, while PV absorbs around 58 % of the solar energy between 200 and 800 nm [42].

A value of one unit or less applies to bulk TE materials at the moment. Studies are being done on materials having zT higher than a unit. A zT value greater than 1 can be achieved using low-dimensional systems, such as NPs. The mid and long-wavelength phonon scattering is affected differently by the structural features of TE materials [43]. Additionally, there are effects on the electrical transport of both hot and cold electrons. It is known that atomic defects can effectively scatter phonons of short wavelengths. Additionally, the electrical transit of both hot and cold electrons is impacted. Atomic defects are capable of scattering phonons of short wavelengths. Nanoparticles (NPs) have been used to increase the zT value. Recent findings have validated the function of grain boundaries in mid- and long-wavelength phonon scattering as shown in Fig. 2. In this Figure, nano-structuring generates a broad density of interfaces that scatter phonons over a wider range than electrons. Consequently, reduces the thermal conductivity of the lattice while maintaining carrier mobility and electronic conductivity. To achieve this, nanostructures can be designed with dimensions smaller than the mean free path of phonons but longer than charge carriers. In general, research into polymers for organic TE materials offers opportunities to create novel and adaptable materials for energy conversion and harvesting applications, with the potential to revolutionize fields like flexible electronics, wearable technology, and sustainable energy generation.

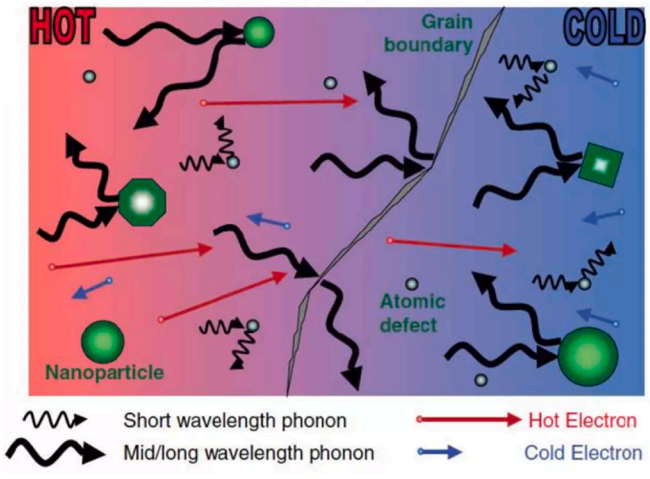

Fig. 2. Schematic illustrating phonon scattering mechanisms via atomic defects, nanoparticles, and grain boundaries [43]. Copyright 2010, Wiley-VCH.

3. Organic thermoelectric materials

On a commercial scale, inorganic crystalline TE materials have ruled all the fields over a comprehensive period till their use was officially banned on account of the highly intrinsically toxic and fragile nature of such materials along with higher costs, relatively heavier weight, and challenging to process further [44]. A general comparison between the properties of organic and inorganic thermoelectric materials is summarized in Table 1.

During the earlier developmental phases, organic materials were underestimated based on their relatively poor TE performance but recent studies were successful in demonstrating the exceptional TE capabilities of polymer-based OTEs analogous to those of conventional inorganic TE materials [45]. Hereby, it has made an attempt in the subsequent sections to summarize the properties, potential research, and fabrication strategies used in organic TE based on polymers.

3.1. Properties of OTE

Doping is usually carried out in conventional inorganic semiconductor materials to alter the compound's band structure by substituting atoms [46]. The combination of suitably selected proper donor and acceptor pairs, charge transfer complexes, or salts can lead to effective OSC doping [47]. Doping is used to improve a material's conductivity by adding more charge carriers (n) and causing the transfer of electrons between the host and the dopant [48]. Redox doping and acid-base doping are principal doping processes in OSCs. Acid-base doping is possible by transferring anions or cations from a dopant to organic semiconductors. However, in the case of redox doping, a donor-acceptor charge-transfer complex or ion pair may be formed as a result of the transfer of electrons that occurs during the redox chemical interaction between the dopant and OSCs. This comprises p-type doping, in which electrons are transported from the semiconductor material's HOMO to the HOMO of the dopant, and n-type doping, in which electrons are transferred from the semiconductor material's HOMO to the lowest unoccupied molecular orbital (LUMO) [49]. Therefore, the dopant and semiconductor molecules' energy levels must match. As a result, adding and subtracting electrons or adding anions/cations are essential ways that polarons are produced. In parallel, a specific segment's aromatic structure is changed into a quinoid conformation and joined with other elements at greater doping levels to create bipolarons and polarons, which are the primary carriers in the majority of OSC materials (Fig. 3).

Table 1
Properties of organic and inorganic thermoelectric materials.

Feature	Organic Thermoelectric Materials	Inorganic Thermoelectric Materials
Thermal Conductivity	Generally lower, beneficial for maintaining a high-temperature gradient	Higher than organic materials
Electrical Conductivity	Lower compared to inorganic materials, but can be optimized through doping and structural modification	Typically higher, advantageous for efficient electrical power generation
Seebeck Coefficient	Comparable to inorganic materials, with significant potential in polymer-based composites	Often high, contributing to their effective power-generation capabilities
Environmental Impact	Often composed of more sustainable and less toxic materials, potentially biodegradable	May contain rare or toxic elements, raising concerns about resource scarcity and environmental harm
Mechanical Properties	Flexible, lightweight, and can be engineered into various shapes and sizes, suitable for wearable technology	Generally rigid, with durability and stability at high temperatures
Cost and Availability	Potentially lower cost due to the use of organic materials and simpler fabrication processes	Cost varies with material scarcity and processing complexity; some materials are expensive and difficult to source

In Fig. 4, OTE metrics for electrical conductivity for a variety of cutting-edge doped organic materials are compiled. For comparison, metrics for standard ambient temperature material, Bi_2Te_3, are provided. The efficiency of OTE materials working near ambient temperature is undoubtedly close to their inorganic counterparts. Understanding the molecular structures and manufacturing processes that resulted in high carrier mobility in OTFTs [51] and high-conductivity electrode layers in OPVs [52] has sped up the development of OTEs. Since many efforts on OTEs have engrossed on maximizing power factor, authors covered the most recent breakthroughs for improving electrical conductivity (σ); this correlates with carrier concentration (n) and the charge carrier mobility (μ) directly. Therefore, both n and μ of a TE material must be kept highest level possible to increase its σ and S values in OTEs, as well as the significance of this research regarding rules for subsequent designs. They additionally investigated the possible effects of increasing the power factor on thermal conductivity, which is heavily influenced by morphology in most materials. It is beneficial to ponder the operation prerequisites for possible ambient temperature TEs, given the extensive range of organic molecular frameworks that are accessible. The electrical conductivities and adjustable charge-carrier concentrations (n) of TE materials must be good [51]. Several OTE materials possess TE properties that follow the same empirical pattern. Since practical TE modules have electrical conductivities of more than 10 Scm^{-1}, or close to room temperature, charge-carrier mobility, and carrier concentration, criteria in organic materials, can be measured. Knowing that molecular density ($n \sim 10^{22}\ cm^3$ in organic systems) limits the carrier concentration, the carrier movement is required to be larger than $0.01 cm^2V^{-1}s^{-1}$ to ensure adequate electrical conductivity at the highest carrier density. According to field-effect conduction, averaged over numerous domains, the mobilities of carriers in organic semiconductors are between 1 and 10 $cm^2V^{-1}s^{-1}$, which is analogous to stated doped bulk values materials [53–55]. Even though it should be emphasized that in the presence of dopant ions, field-effect mobility computed at a dielectric interface in a thin-film transistor may not match bulk mobility, the similarity of the results suggests that it serves as a credible reference. The requirements for electrical conductivity can be determined in parts by metrics like mobility, but the dependency of S on carrier concentration is challenging to calculate for many materials, making it the highest undefined factor for organic materials.

3.2. Materials for OTEs

Organic TE (OTE) materials come in many different forms, each with unique properties, advantages, and potential applications. These substances typically include organic compounds with TE characteristics or polymers. Typical examples of organic TE materials include the following: conducting polymers, small organic molecules, organic-inorganic hybrid materials, covalent organic frameworks (COFs), conjugated polymers, carbon-based materials, polymer blends, and composites, metal-organic frameworks (MOFs), organic nanowires and nanotubes, polymer-nanoparticle composites, polymer-carbon nanotube composites, and ionic conducting polymers.

The ideal TE performance, economic considerations, processing techniques, and application requirements all play a role in selecting the best type of OTE material. To advance organic TE technology and its potential uses in energy harvesting, waste heat recovery, and environmentally friendly electronics, researchers are constantly investigating and creating new materials and architectures.

There are several compelling factors to investigate polymers as organic TE materials because of their distinctive features and prospective applications. Here are some explanations for why scientists are drawn to studying polymers in this situation: flexibility and processability, low thermal conductivity, tunable electrical properties, low cost

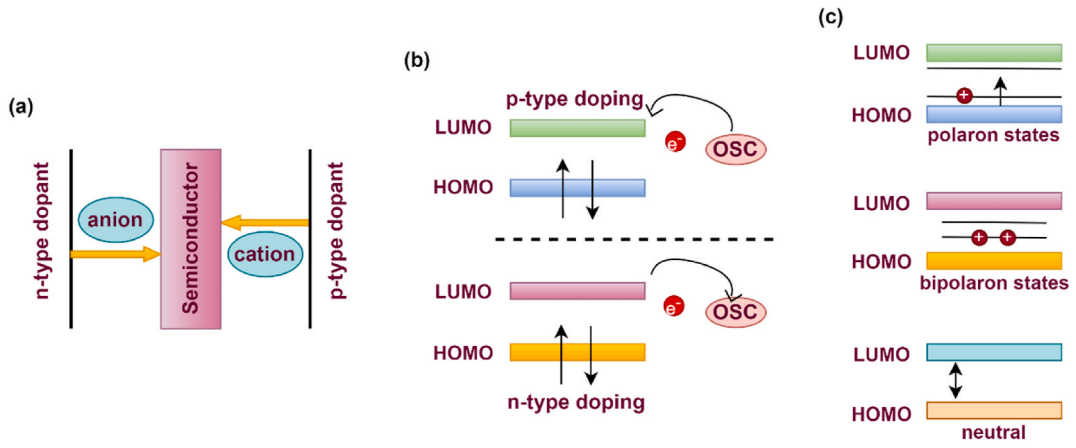

Fig. 3. (a) Doping via anion and cation transport. (b) p-type doping of semiconductor for electron transfer from OSC to dopant and n-type doping of electron transfer from dopant to the semiconductor. (c) Alteration in electronic configuration and polaron states.

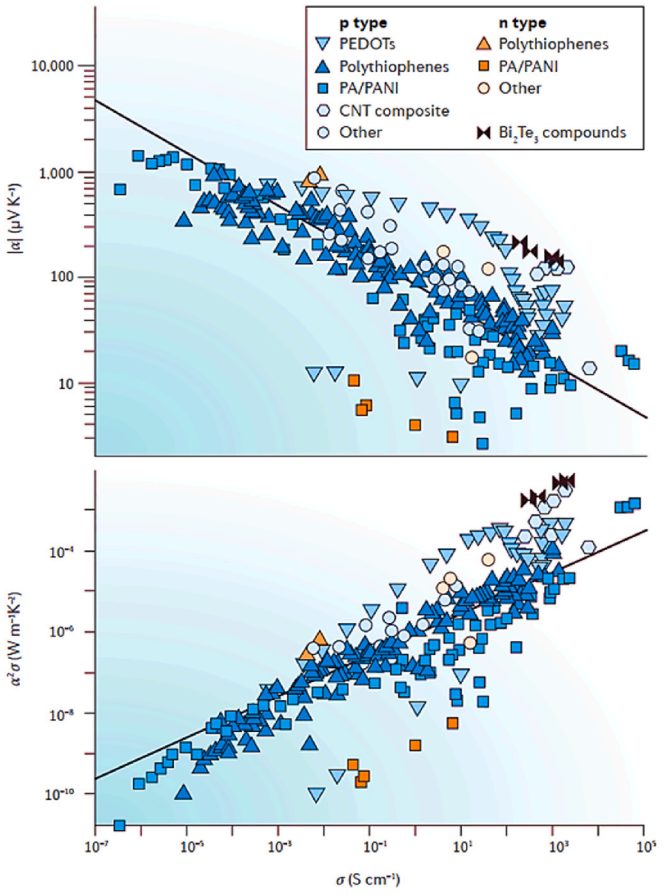

Fig. 4. OTE materials follow the same trend of TE properties for PEDOT, PA, PANI, CNT composites, and other organic molecules. Bi_2Te_3 (best inorganic compound) is selected as a reference [50]. Copyright 2016, Nature.

and scalability, lightweight nature, mechanical durability, compatibility with fabrication techniques, integration into flexible and wearable electronics, reduced environmental impact, exploration of new material chemistries, multi-functionality, customizable thermal stability.

In conclusion, research on polymers for organic TE materials offers opportunities to create novel and adaptable materials for energy conversion and harvesting applications, with the potential to revolutionize fields like flexible electronics, wearable technology, and sustainable energy generation. Due to the reasons mentioned, this review focuses on polymer-based OTEs.

3.3. Polymer-based OTE material

The polymers used in OTEs can be categorized into two classes: conducting/non-conducting or p-type/n-type polymers. The conducting polymer, especially p-type owing to its intrinsic charge conduction properties, is more preferred for employment in the practical TE world [56]. However, the non-conducting and n-type polymers impede the bundle-bundle hopping phenomenon, causing a significant reduction in their relative TE performances [57]. Examples of conducting polymers include polyacetylene (PA) [58], polythiophenes (PTh) [59], poly(3, 4-ethylenedioxythiophene) (PEDOT) [60], poly(3-methylthiophene) (P3MT) [61], etc. while some of non-conducting polymers are polyvinylidene fluoride (PVDF) [62], poly(3-octylthiophene) (POT) [63], and poly(3-hexylthiophene) (P3HT) [64]. Fig. 5 demonstrates the molecular structure of some p-type and n-type polymers.

p-type OTE materials have drawn more interest and helped to achieve several important developments in molecular design, TE conversion processes, and device fabrication. They still have a restricted variety of molecular system types, low doping stability, and inadequate performance. Several molecular design research has focused on these unsolved issues (Fig. 6) [65].

PEDOT, a renowned TE polymer based on the monomer ethylenedioxythiophene (EDOT), is a widely researched p-type conducting polymer due to simple oxidative polymerization in H_2O, as well as its air-stable and water-processibility properties, which are advantageous for commercial applications [66–68]. Its polystyrene sulfonic acid (PSS) doped variant produced the highest zT (at RT) in organic TEs in an OTEG. Wen et al. successfully exhibited ultra-flexible PEDOT: PSS fibers-based OTEG with a high PF of 147.8 $\mu Wm^{-1}K^{-2}$ for μm scaled conducting polymers with an electrical conductivity of 4029.5 Scm^{-1} following post-treatment with H_2SO_4 [69]. Ouyang et al. significantly increased σ of PEDOT: PSS from 0.3 to 3065 S cm^{-1} following treatment with 1 M H_2SO_4 [70], and their transparency can be comparable to ITO electrodes. In 2014, Lee et al. developed solution-processed, highly conductive, and stable PEDOT: PSS nanofibrils [71]. A charge-separated transition state allowed for the rearrangement of the H_2SO_4 PEDOT: PSS structure into highly organized and densely packed nanofibrils (Fig. 7). Aside from acid treatment, polar organic solvents such as dimethyl sulfoxide (DMSO) and ethylene glycol (EG) were demonstrated to be effective [72–74], and ionic liquids [75,76] can strengthen TE properties of PEDOT: PSS [77]. Liu et al. reported increased π-π stacking PEDOT: PSS hydrogel fibers treated with sulfuric acid and organic solvents, providing a PF of 4.77 $\mu Wm^{-1}K^{-2}$ [78].

Polyaniline (PANI) is one more p-type conductive polymer that is

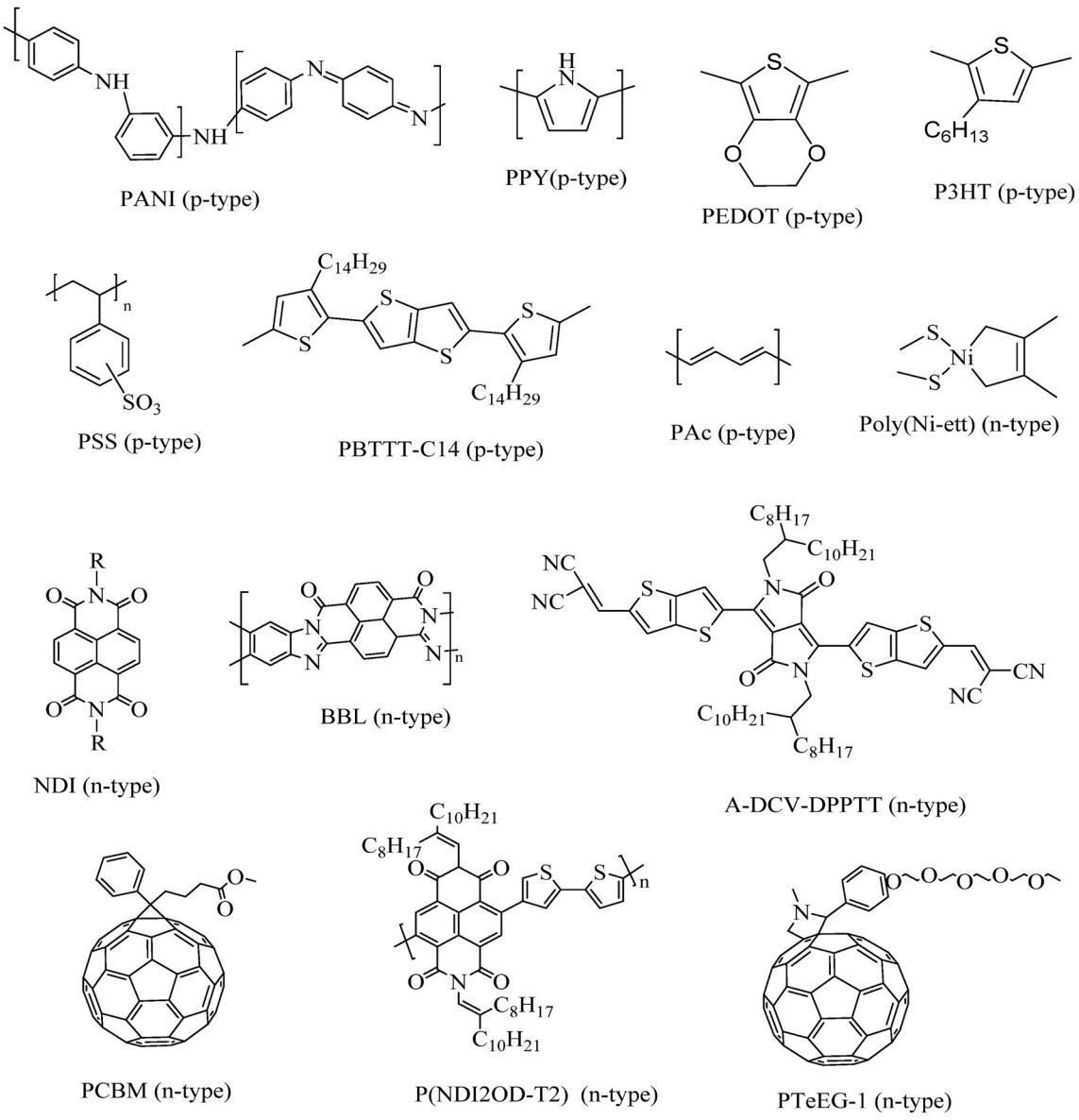

Fig. 5. Molecular structure of some p-type and n-type polymers.

extensively utilized in commercial sectors due to its ease of synthesis, thermal and chemical stability, and application in the development of OTEG [79–82]. PANI was acid-doped (HCl, camphor sulfonic acid (CSA)) to achieve conductivity beyond 5700 Sm^{-1} [83], enhancing *PF* and electrical conductivity [77,84]. Furthermore, a composite of PANI and SWCNT with partial de-doping demonstrated a high *PF* of 345 $\mu Wm^{-1}K^{-2}$ [85]. TE properties were similarly improved by using A-CNT/PANI (A-CNT: amine-functionalized SW/DWCNT) composites, leading to conductivities up to 2012 Scm^{-1} and *PF* of 400 $\mu Wm^{-1}K^{-2}$, improved from 273 $\mu Wm^{-1}K^{-2}$ after fine-tuning the CSA ratio [86]. Toshima et al. explained the inclusion of Bi_2Te_3 inorganic nanoparticles into a camphor sulfonic acid-doped PANI solution [87].

Poly(3-hexylthiophene-2,5-diyl) (P3HT) is an n-type conductive polymer studied in organic electronics and basic mechanisms in TEs such as structure-dopant interactions. Kang et al. demonstrated double doping of P3HT in ambient air with $AuCl_3^-$ and Au nanoparticles, resulting in σ of 207 Scm^{-1} and a *PF* of 110 $\mu mWm^{-1}K^{-2}$ [88]. Gregory et al. analyzed the TE properties of thin films of poly (3-alkylchalcogenophene) in conjunction with heteroatoms and doping methods [89]. The study examined three distinct heteroatoms with an alkyl solvating group: S (thiophene), Se (selenophene), and Te (tellurophene). As a result, electrical conductivity increased with heavier heteroatoms from S to Se to Te, whereas thermopower increased in a reverse direction.

Polymers based on naphthalene diimide (NDI) are a further kind of n-type non-conductive polymers with potential effectiveness for TE applications due to their elevated electron affinities and self-dopable structures obtained by hitching a particular group to conjugated backbone [90–94]. The effects of various alkyl spacer lengths inside the backbone and charged side groups were investigated by Russ et al. [95]. They achieved a *PF* of 1.4 $\mu Wm^{-1}K^{-2}$ by combining a charged doping group linked to a conjugated backbone and suitable side chain length. Poly([N,N0-bis (2-octyldodecyl)naphthalene-1,4,5,8-bis(dicarboximide)-2,6 bis(dicarboximide)-2,6-bis(dicarboximide)-2,6-bis(dicarboximide)-2,6-bis(dicarboximide)-2 diyl]-alt-5,50-(2,20-bithiophene)) (P(NDI2OD-T2), also known as N2200, is commonly doped with dihydro-1Hbenzoimidazol-2-yl (N-DBI) derivatives (i.e. N-DMBI, N-DPBI) and has electrical conductivities in the range of 10^{-3} Scm^{-1} [96,97]. Alkyl chains were substituted with polar triethyleneglycol-based ones by Liu et al. to boost miscibility, and following N-DMBI doping, they obtained an electrical conductivity of

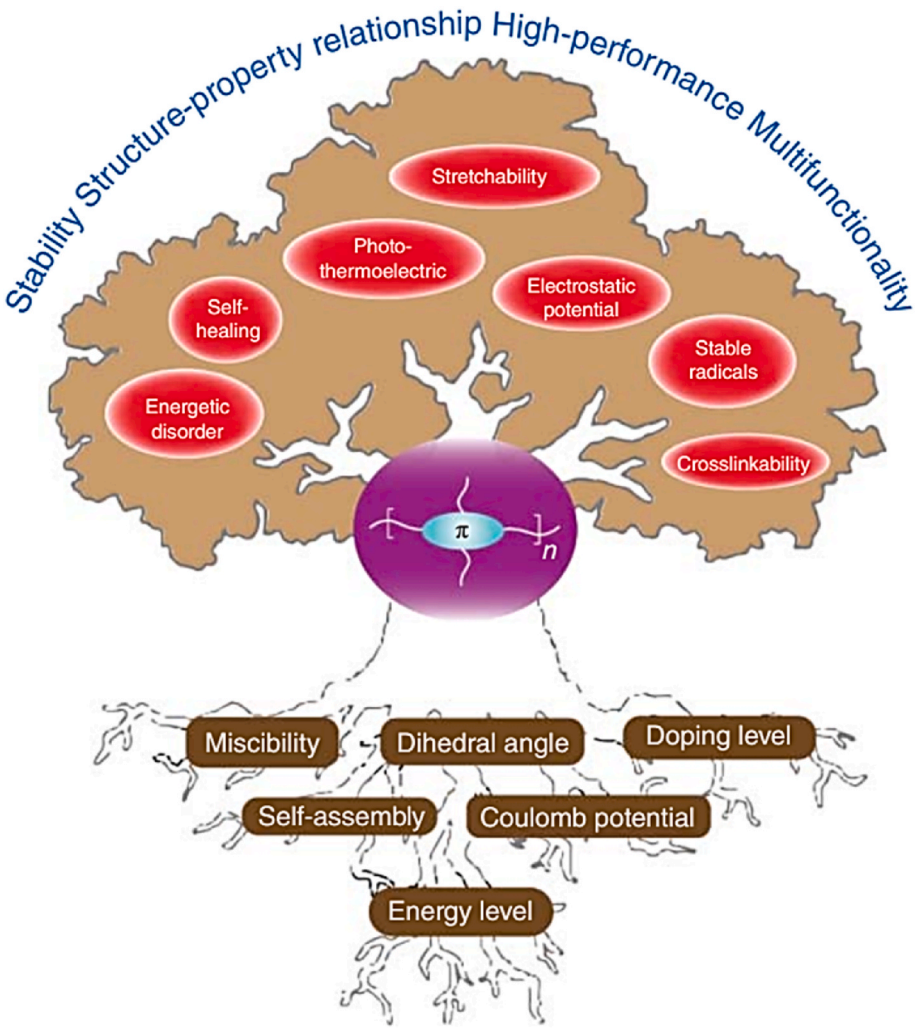

Fig. 6. The molecular design concepts for OTE materials [65]. Copyright 2021, Chinese Chemical Society Publishing.

0.17 Scm^{-1} [98]. According to Wang et al., replacing the bithiophene (T2) unit with the more electron-deficient bithiazole (Tz2) unit, P (NDI2OD-Tz2), increased the stiffness and planarity of the backbone while also improving the electron affinity, which led to more effective doping and improved TE properties (*PF* of 1.5 $\mu Wm^{-1}K^{-2}$) [99].

Huang et al. stated unique small molecule called (aromatic-dicyanovinyl-dipyrrolo [3,4-c] pyrrole-1,4-diylidene) bis (thieno [3,2-b] thiophene (A-DCV-DPPTT)), which after being doped with N-DMBI generated an electrical conductivity of 5.3 Scm^{-1} and a zT value of 0.11 ± 0.01 (at RT) increased to 0.23 ± 0.03 (at 100 °C) indicating no increase in π-π stacking distance after doping [100]. Fullerenes' high electrical conductivity and low heat conductivity make them ideal candidates for n-type TE materials. Doping fullerenes with cesium carbonate (Cs_2CO_3) (C_{60}/Cs_2CO_3) results in *PF* of 28.8 $\mu Wm^{-1}K^{-2}$ [101]. A material wherein the electron mean free pathways are as long as feasible and the phonon mean free paths are as minimal as probable is referred to as a "phonon-glass electron crystal" and when PTEG-2 was doped with N-DMBI obtained electrical conductivity of 410 Scm^{-1} and $zT = 0.34$ (at 120 °C) [102,103]. Fullerene derivatives with lateral double-triethylene-glycol side chains showed better doping and thermal stability. In fullerene derivatives, the significance of the side chain's polarity (alkyl vs polar ethylene glycol) was also investigated. A *PF* of 23.1 $\mu Wm^{-1}K^{-2}$ was attained on a specific derivative (PTeEG-1) as an outcome of increased molecular packing and doping efficiency [104].

Zuo et al. investigated inverse-sequential doping approach on [6,6]-phenyl C_{61}-butyric acid methyl ester (PCBM) with N-DPBI, and it resulted in extremely high electrical conductivity of ~40 S m^{-1} and *PF* of 35 $Wm^{-1}K^{-2}$ in comparison to bulk doped version with ~6 S m^{-1}, *PF* ~3 μW m^{-1} K^{-2} correspondingly [105]. A unique n-type ink that has recently been developed has excellent conductivity (reaching 8 S cm^{-1}), making it attractive for the continued progress of OTEGs [106]. Distinctive n-type conductive ink is an ethanol-based mixed ion electronic conductor with strong ambient, thermal, and solvent stability. It is composed of poly (benzimidazobenzophenanthroline): poly(ethyleneimine) (BBL:PEI). Printable BBP-PEI ink (BBL: PEI (33 wt% PEI_{lin}) combined with PEDOT: PSS, provides the maximum power output per thermocouple for all-polymer TEGs in-plane. The metal connection and power output are noteworthy. Table 2 represents the TE properties of different representative conjugated polymer-based TE materials without nano inclusions.

Nonetheless, any further development based on OTEs has been neglected based on lower charge carrier's concentration which further corresponds to a low *PF* value and *S* [113]. On further comparison, it was confirmed that the conventional inorganic TE materials exhibit *PF* three times that of OTEs [114], so the researchers started practicing an approach of growing polymer-based organic–inorganic TE composites to combine both of their properties explicitly, which yielded reasonably satisfactory results over time [115].

3.4. Fabrication strategies

Organic semiconductors (especially conjugated polymers) are

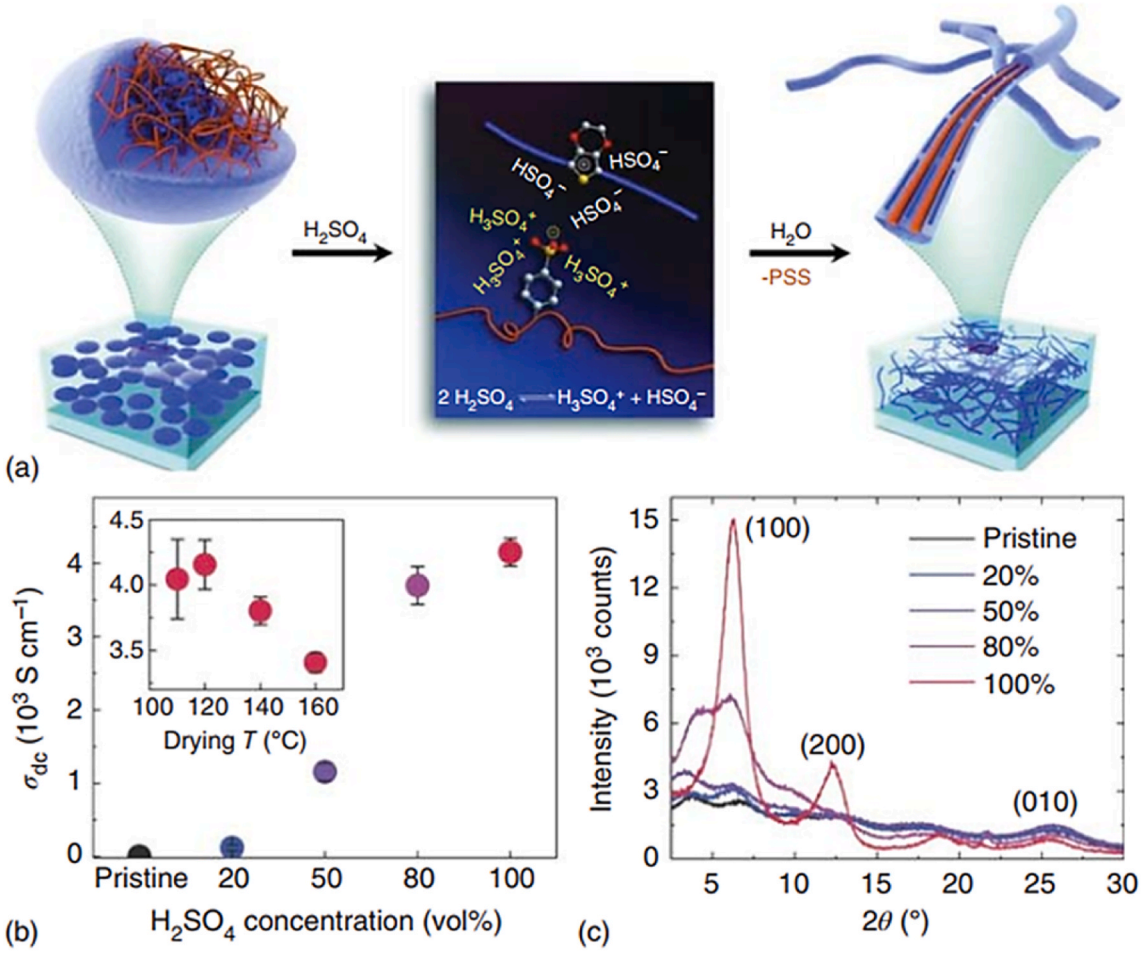

Fig. 7. (a) illustrates the structural rearrangement of PEDOT: PSS after a post-treatment with concentrated H_2SO_4. (b) The association between the pH and the concentration of H_2SO_4. (c) An XRD pattern of films made of PEDOT: PSS at various H_2SO_4 concentrations [71]. Copyright 2013, Wiley-VCH.

Table 2
A summary of polymer-based OTEs.

Polymer	Preparation method	σ (S/cm)	S (μV/K)	κ (W m^{-1} K^{-1})	zT (T)	Temperature (K)	Ref.
Polyacetylene	Casting	4.990–11.560	11.4–28.4	0.7	0.0047–0.38	300 K	[107]
Polypyrrole	Casting	100	12	0.1–0.2	0.002	300 K	[107]
Polyaniline (PANI)	Casting	7.000	7	0.1–0.2	0.051	300 K	[108]
Polythiophene	Casting	100	21	0.1–0.2	0.0066	300 K	[109]
Poly(*para*-phenylene)	Casting	10^{-5}	12	0.1–0.2	2.1×10^{-10}	300 K	[110]
Poly(*p*-phenylene vinylene)	Casting	10^{-5}	7	0,1–0,2	$7{,}2 \times 10^{-11}$	300 K	[111]
Poly(carbazolenevinylene)	Casting	5×10^{-3}	230	0.1–0.2	8×10^{-5}	300 K	[110]
PEDOT: PSS	Casting	55	13	0.1–0.2	0.0014	300 K	[112]

adaptive to chemical modification in their structures and possess good solubility in various solvents [116]. There are many fabrication approaches reported to date, which include spin coating, inkjet printing, spray coating, screen printing drop-casting, etc. [117,118], as illustrated in Fig. 8.

Spin coating is typically designed for the deposition of thin layers of organic semiconductors mainly if uniform thickness is critical for device performance [119]. Spin coating is the most often used deposition process for PEDOT: PSS [120]. A single layer of spin-coating is typically 100 nm thick. Spin-coating is a method of coating a solution that contains both the EDOT monomer and its oxidant, iron (III) tris-*p*-toluenesulphonate. Yvenou et al. examined ultrasonic spray-coating of PEDOT: OTf with 156 thermocouples using oxidant iron (III) trifluoromethane sulfonate, achieving a power output of 1 μW with a 48 °C temperature differential [121]. Elmoughni et al. investigated a very practical textile integrated organic TEGs, demonstrating a 32-leg device manufactured from PEDOT: PSS (p-type) and poly[Na(NiETT)] (n-type) inks, with a $V_{oc} \approx 3$ mV, at $\Delta T = 3$ K [122]. They proposed that a 1072-leg prototype might generate 13 μW from a 3 K temperature alteration in the body [123]. Contrarily, the OTEG prototype made with carbon nanotube (CNT) inks, exhibited a remarkable power production of 342 μW at $\Delta T = 150$ K on printable all-carbon materials without any metallic junctions.

Drop-casting is a viable technique for fabricating layers up to 10 mm thick [124]. Polypyrrole (PPy) is another conjugated polymer that is commonly used in the development of OTEG. PPy thin films are typically produced via electrochemical synthesis in a three-electrode setup at room temperature. Throughout the same year, Wu et al. described an alternative method for fabricating PPy nanotubes [125]. These nanotubes may be effectively diffused in ethanol and placed in glass petri

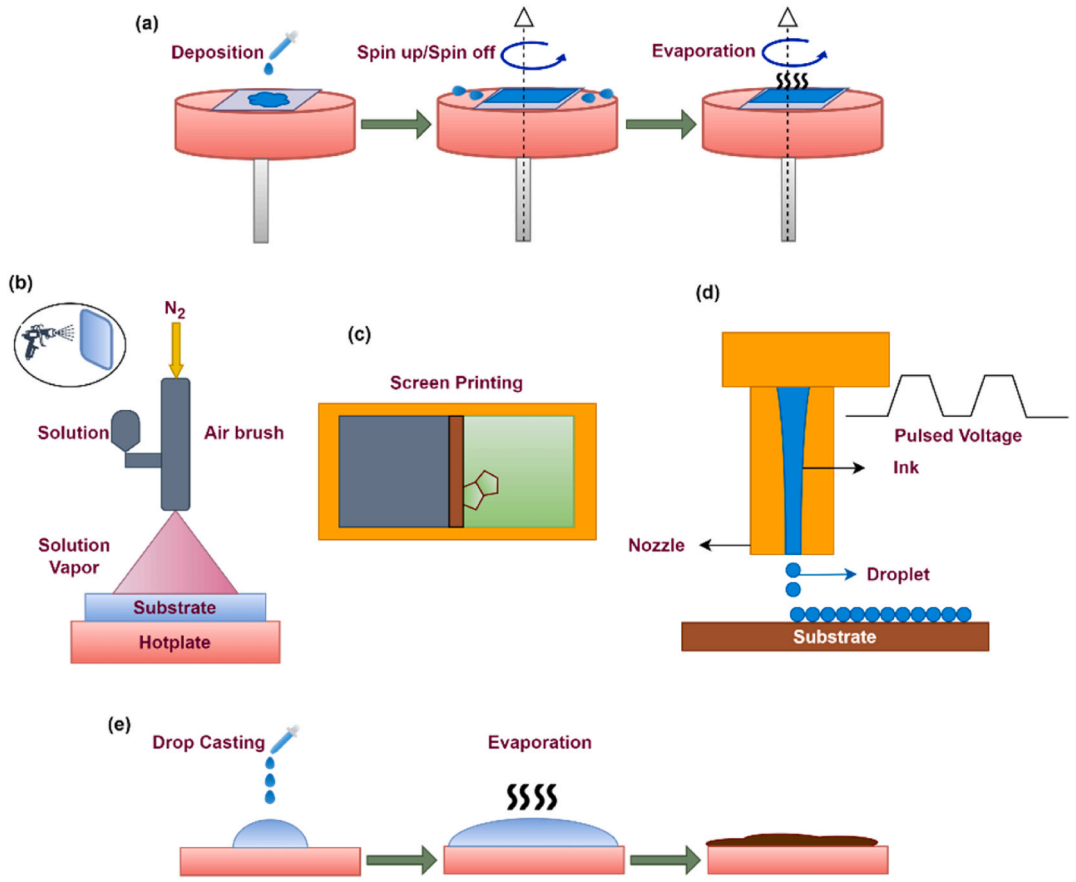

Fig. 8. Fabrication strategies for TE devices (a) spin coating (b) Spray coating (c) Screen printing (d) Inkjet printing (e) drop casting.

plates, according to this study. The nanotubes form manageable sheets after the ethanol evaporates. Wang et al. created PPy/graphene composite nanosheets using an in situ chemical oxidative polymerization process, which was then cold-pressed into pellets [126]. In this instance, PPy nanotubes were made using multi-walled carbon nanotubes (MWCNT) as templates. According to Yao et al., single-walled carbon nanotubes (SWCNT) were utilized as templates to generate thin layers of PANI [127]. The synthesis was carried out using a suspension of aniline, SWCNT, and an oxidant agent. Precipitate was subsequently purified, washed, and pressed. Zhang et al. reported an analogous strategy that used MWCNT as an alternate to SWCNT [128]. Zhao and colleagues demonstrated another PANI-based composite material by dispersing graphite oxide (GO) particles in an aqueous solution having an oxidant agent and aniline precursor [129].

Polythiophenes are a further class of p-type conjugated polymers that are commonly employed in the development of OTEGs [130]. Poly-(3-hexylthiophene) (P3HT) is the most frequently referred polythiophene, owing to its commercial availability and ease of dissolution in a wide range of solvents. P3HT is almost always chemically doped when used in TE systems because its immaculate electrical conductivity (108 S cm^{-1} at ambient temperature) [131] hinders effective thermal conversion. For optimal chemical doping of P3HT, various molecules have been reported. As a doping substance, Zhang et al. chose a ferric salt of a trifluromethanesulfonimide anion $(CF_3SO_2)_2N^-$ [132], whereas Xuan and colleagues used nitrosonium hexafluorophosphate/acetonitrile [133]. Lately, OTEG was effectively fabricated using a unique category of composites developed by combining P3HT with carbon-based materials. To make a solid film, two deposition processes were used: drop casting on a bare substrate followed by spray coating with a shadow mask. The printed layer shape (a greater number of inter-CNT bundle connections) is credited with the improved TE performance of spray-coated films, according to the studies.

Lee et al. proposed a composite material that was identical. SWCNT (at various concentrations ranging from 30 to 60 % wt) was added to the P3HT solution dispersed in o-dichlorobenzene to generate the dispersion [134]. Yet again, wire-bar coating and drop-casting were used as deposition techniques. The greater density of SWCNT bundles in bar-coated films led to superior TE performances. They also demonstrated how spin-coating $FeCl_3$ solution in nitromethane over top of dry layers can improve the TE response of their composite.

Poly-(2,5-bis(3-alkylthiophen-2-yl) thieno [3,2-b] thiophene] (pBTTT) is another famous polythiophene polymer [135]. In a fascinating study, Venkateshvaran et al. used pBTTT as the active layer in a transistor design [136]. The examination of spin-coated thin films demonstrates that the Seebeck coefficient is influenced by the applied gate voltage. Even though the most effective topologies need the inclusion of both types of semiconductors, n-type semiconductors are significantly less typically reported in OTEG production than their p-type counterparts [137,138]. The finding might be caused, at least in part, by the low ambient stability that has previously been associated with n-type OSCs. The drop-cast technique, which produces a multicomponent film by alternately dropping a polymer dispersed in a solution onto a substrate, is one of the simplest ways (Fig. 9a) [139]. This technique effectively increased TE and enabled control of layer thickness. As the deposition potential, deposition period, and electrolyte ion concentration could be easily adjusted, electrochemical polymerization could control the level of oxidation and thickness of conducting polymers. On CNTs, conducting polymer nanostructures were electrochemically deposited using electrostatic attraction and π–π stacking. The monomers polymerized over the surface of the SWCNTs when the oxidant ammonium persulfate was introduced to the suspension,

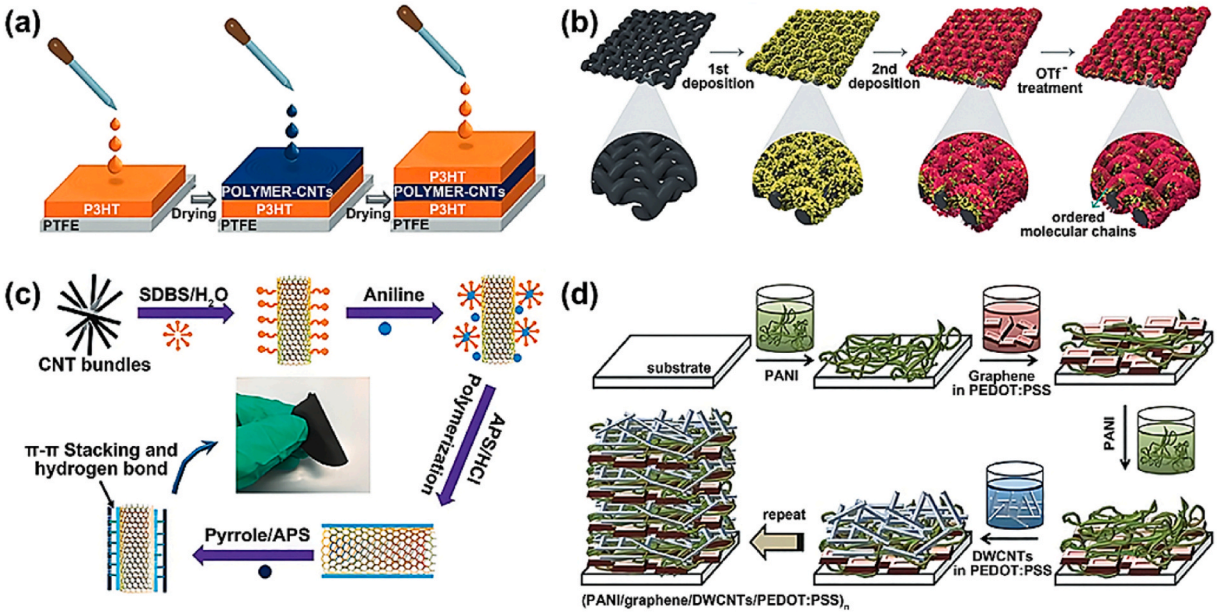

Fig. 9. Three-component composites are often prepared using standard techniques. (a) drop-casting technique [139]. Copyright 2021, Informa UK Limited. (b) Electrochemical deposition [142]. Copyright 2021, Royal Society of Chemistry. (c) In situ method [140]. Copyright 2020, Royal Society of Chemistry. (d) LBL assembly [141]. Copyright 2016, Wiley-VCH.

enabling the adequate preparation and adsorption of PANI nanoparticles. A ternary composite was created by tightly wrapping the PPy layer around the surface of the PANI/SWCNT binary composite after the pyrrole monomer had been introduced (Fig. 9c) [140]. Layer-by-layer (LBL) assembly is an effective technique for creating multi-component composite TE materials. The spontaneous association between layers will result in molecular aggregates of ordered structures, either as a result of strong interactions or weak interactions between the molecules of each layer (like electrostatic attraction, hydrogen bonds, coordination bonds, etc.). Owing to its simplicity, low cost, abundance of film-forming materials, high order, and controlled thickness, LBL assembly technology exhibits unique benefits. Additionally, the system's transport performance might be significantly enhanced by a 3D carrier transport network built between various levels (Fig. 9d) [141].

Current advances in the synthesis of substantially more air-stable n-type polymers have significantly increased the number of papers about this specific class of material [143]. Soluble fullerene derivatives are a significant class of n-type semiconductors used in the fabrication of OTEG. These materials usually need to be manufactured in conjunction with chemical dopants because of their extremely low electrical conductivity at room temperature (108 Scm^{-1}) [144]. Zuo and colleagues proposed two distinct doping techniques for thin films of [6,6]-phenyl-C61-butyric acid methyl ester (PCBM) [145]. Before spin-coating, the dopant, 4-((1,3-dimethyl-2,3-dihydro-1H-benzoimidazol-2-yl) phenyl) dimethylamine (n-DMBI), was added straight into PCBM solution. The second approach (known as inverse-sequential doping) involved spin-coating the substrates using a solution comprising only of a semiconductor that had previously been doped solely with the dopant. Better results (in terms of the *S* and *PF*) were obtained using this second strategy. Liu et al. reported yet another fullerene derivative. The authors created a variety of fuller pyrrolidines with various lengths of oligo-ethylene glycol side chains or n-dodecyl side chains as the alkyl side chains [146]. These semiconductors were doped with n-DMBI via spin-coating, and they were dissolved in chloroform. Mainly, a fascinating aspect of this study is the in-depth analysis of how polarity and length of side chains affect TE performances. The key conclusion is that the two factorsrequire vigilant optimization to achieve high molecular order, which is critical for improving OTEG performance. They recently reported a new fullerene-derived material, which they utilized to create a "phonon-glass electron-crystal" (PGEC) like organic TE material, doped with n-DMBI and deposited by spin-coating [147].

Since their simplicity in liquid phase processing, OSCs are excellent candidates for device fabrication using printing techniques [148]. However, for OTEG, the number of systems and printed devices reported till now has been remarkably low. Inkjet printing seems to be the one that fabricates TE systems the most frequently out of all printing techniques. By using inkjet printing, Bubnova et al. reported creating OTEGs from a PEDOT derivative called PEDOT: tosylate using a liquid containing both EDOT monomer and oxidant molecule $Fe(Tos)_3$ [149]. Hong and his coworkers also used spray coating [150]. They talked about how a flexible polyimide substrate was coated with a chloroform-dispersed CNT-P3HT nanocomposite. Yang et al. published the synthesis and characterization of a novel ethanol-based n-type semiconductor developed using conjugated polymer poly(benzimidazobenzophenanthroline) (BBL) nanoparticle dispersions in poly(ethyleneimine) (PEI) [151]. While PEDOT: PSS (doped with DMSO) was introduced into the active material to create p-type legs of an OTEG, this inkjet printable hybrid material was employed to create n-type legs of the device. The creation of OTEGs has successfully utilized both inkjet printing and screen printing. Wei and his partners announced a TE generator made entirely of cellulosic substrates that were screen-printed [152]. The TE material was PEDOT: PSS and the electrical contacts were made with a conductive silver paste. The innovative method put forward by Sndergaard et al. combined flexography and screen printing [153]. Electrical connections were created using conductive silver paste and PEDOT: PSS as the active material. We et al. showed a hybrid organic/inorganic system [154]. This device was developed by screen-printing an inorganic semiconductor layer (Bi_2Te_3 (n-type) and Sb_2Te_3 (p-type)) followed by coating it with a drop cast layer of PEDOT: PSS. PEDOT: PSS has been eliminated from the substrates by spinning them at high rotational speeds, allowing the organic layer to create a matrix containing inorganic semiconductors. Finally, Kee and colleagues detailed 3D-printed TE devices [155]. The studies revealed a stretchable, self-healing ternary compound made of DMSO (added to improve TE capabilities), PEDOT: PSS mixed with a polymeric surfactant, Triton X-100 as a healing agent, and PEDOT: PSS. Devices with 10 legs that were electrically and thermally connected in parallel and series, respectively, were 3D-printed using the composite.

4. Potential composites

4.1. Carbon nanotube based OTE

Carbon materials are considered naturally bestowed with incredible electrical conductivity potential and are widely used in TE applications [156]. Carbon nanotubes (CNTs) further cause the conductivity enhancement of their composites as well. The electrical conductivity of CNTs combined with PEDOT-Tosylate exceeds 1000 Scm^{-1}, and *PF* of 35 $\mu Wm^{-1}K^{-2}$ has been observed [157]. Decoupling the σ and *S* also takes into account the properties of carbon-based TE materials. Prepared composites, however, exhibit a low thermal conductivity due to the scattering of phonon mechanism occurring at their carbon-polymer interfaces, thus making such materials commercially viable and more effective, owing to high environmental competencies and reliability as well.

CNTs exhibit an exclusive 1-D structure called Single Walled CNTs (SWCNTs) are attractive conducting materials due to their fabrication as the 1-D TE nanomaterials, theoretically, demonstrate better performances than multidimensional materials [158]. Furthermore, their TE efficiency can be enhanced by rising charge mobility along the larger axis, or by decreasing the diameters to lessen the respective thermal conductivities [159]. PEDOT: PSS particles painted on the surface of the CNTs are electrically conductive and prevent heat transfer due to different bonding and vibrational spectra between the CNTs and PEDOT: PSS, as illustrated in Fig. 10A, which is the proposed charge transport mechanism [160]. As a result, the thermal conductivity was still on par with that of polymers. The decoupling of electrical and thermal transport features dramatically raised the *PF*. Fig. 10B depicts σ and *S* of the composites at different CNT concentrations. A maximum power factor of 100 $mW/m^{-1}K^{-2}$ is observed at a 60 % weight percent CNT concentration [160].

On comparison of CNTs with organic polymers, it was found that the former exhibits an extreme mobility of 100000 cm^2/Vs with thermal conductivity of 3000 $Wm^{-1}K^{-1}$, while the latter possesses a 50 cm^2/Vs carrier mobility with minimum thermal conductivity of 0.2 $Wm^{-1}K^{-1}$ [161]. Owing to possessing holes as the primary charge carriers, CNTs are usually considered p-type TE materials [162]. The n-type analogous were non-existent until Bradley, in 2000, discovered that the CNTs show n-type TE properties under vacuum ambiance, thus suggesting pristine CNT as an intrinsic n-type TE material [163]. Their further research proved that the Seebeck value is dependable on ambient oxygen concentration, thus introducing the possibility of conversion from semiconductor to metallic nature of CNT via exposure. This p-to n-type transition has now expanded its research and possible application scope to the scientific and industrial fields. Moreover, the semiconductor CNT with different dopants, in an atmospheric ambiance also depicts n-type TE performances. Table 3 lists the TE outcomes of CNT-based organic TE materials.

4.2. Graphene

Graphene, is deemed as a burgeoning 2-D crystalline TE material, possessing a remarkably huge value of electrical conductivity along with satisfactory TE performance [172]. The high electrical and thermal conductivity, stability, and scalability of graphene polymer composites make them superior to others for use in TE devices [173]. Table 4 summarizes TE results of OTE materials based on graphene or graphite. Among the artificially-synthesized intercalated graphite compounds, expanded graphite is quite important to mention here. It consists of a 3-D structure that expands on heating and bears significantly higher electrical and thermal conductivities. This material was typically utilized for thermal management applications. Pan et al. obtained a Polyaniline (PANi), expanded graphite composites having enhanced TE performances by using ultrasonic mixing methodology [174]. The fabricated composites bear interesting structures: when polyaniline was introduced into expanded-graphite sheets, the obtained material demonstrated a sandwich structure. On increasing the concentration of expanded graphite in this compound, σ, and *S* seemed to grow as well; therefore, via using this approach, the maximum obtained *PF* was reported to be 2.43 $\mu Wm^{-1}K^{-2}$. Thus, from this discussion, it is fair to conclude that graphene or CNT-based OTEs, in terms of TE performances, are way superior to either graphite- or expanded-graphite-based OTEs. Therefore, its commercialization and further research on practical applications have been constrained.

4.3. Ternary composites

Ternary composites, for instance, PEDOT: PSS/SWCNT/Te nanocomposites, PEDOT: PSS/rGO/Te nanowires, and polypyrrole/graphene/PANi, have widely been investigated because of their outstanding synergistic effect among different constituents and unique internal structures [183]. Cho et al. experimented layer-by-layer approach to fabricate printable TE composites constituted from graphene, double-walled CNT (also DWNT), and PANi material where graphene and DWNT were stabilized via highly conductive PEDOT: PSS film [184]. The triple layered structures of PANi/DWNT-PEDOT: PSS, PANi/graphene-PEDOT: PSS/PANi/DWNT-PEDOT: PSS, and PANi/graphene-PEDOT: PSS thus obtained, have shown an increase in corresponding electrical conductivities on the increased number of cycles. Among these materials, PANi/graphene-PEDOT: PSS/PANi/DWNT-PEDOT: PSS demonstrated maximum σ, i.e. 1885 Scm^{-1} at 80 quad layers, thus indicating the formation of an enhanced interconnected channel for electronic transmission [185]. The p-type *S* was found to be a function of several cycles and the *S* value of both composites, i.e. PANi/graphene-PEDOT: PSS and PANi/DWNT-PEDOT: PSS, amplified with layer cycles, consequently, reaching 58 and 92 μVK^{-1}, correspondingly. PANi/graphene-PEDOT: PSS/PANi/DWNT-PEDOT: PSS composite film also demonstrated the same relation regarding *S* value and, therefore, at 80 quad layers, reported a value of 120 μVK^{-1}.

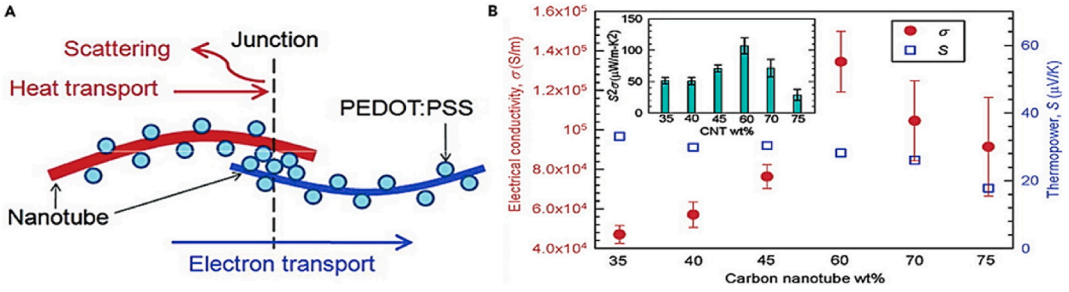

Fig. 10. PEDOT: PSS-CNT nanocomposites' electrical characteristics The connections of CNTs covered with PEDOT: PSS particles are depicted schematically in (A). Instead of creating advantageous paths for electrons, the junction is supposed to prevent the transfer of heat. (B) At various CNT concentrations, the composites' σ and *S*. There is a TE power factor insert [160]. At a 60 wt% CNT concentration, a maximum *PF* of 100 $mW/m^{-1}K^{-2}$ is seen. with Yu et al.'s permission; modified [160]. Copyright 2011, American Chemical Society.

Table 3
A summary of TE results of CNT-based organic TE materials.

Materials	Preparation Method	Seebeck Coefficient (μVK^{-1})	Thermal Conductivity ($Wm^{-1}K^{-1}$)	Electrical Conductivity (Scm^{-1})	Power Factor ($\mu Wm^{-1}K^{-2}$)	zT	Temperature (K)	Ref.
SWCNT	Doping with KOH	−63	0.124	69	27	0.07	–	[164]
PANI/SWCNT	Casting Suspension	65	0.43	769	176	0.12	–	[165]
PANI/MWCNT	Spark Plasma Sintering	25	0.18–0.79	159	0.1	7.6×10^{-5}	300 K	[166]
PEDOT: PSS/ graphene/ MWCNT	In situ polymerization	23.2	0.36	689	37.08	0.031	300 K	[167]
P3HT/MWCNT	Solution based	27	–	27.5	2	8.71×10^{-4}	393 K	[168]
PEDOT: PSS/ SWCNT		19	0.53	4000	140	0.03	300 K	[169]
MWCNT/PPy		25		35	2	–	–	[170]
MWCNT/P3HT	Solution mixing	27		27.5	53	8.71×10^{-4}	393 K	[171]

Table 4
TE results of organic TE materials based on graphene or graphite.

Materials	Preparation Method	Seebeck Coefficient (μVK^{-1})	Electrical Conductivity (Scm^{-1})	Power Factor ($\mu Wm^{-1}K^{-1}$)	Temperature (K)	Ref.
PEDOT/graphene	Solution dispersion	17	1160	33	293 K	[175]
PEDOT: PSS/graphene	in situ polymerization	27	637	46	–	[176]
PANi/rGO	in situ polymerization	24	3677	214	420 K	[177]
PEDOT/graphene/C60	solution dispersion	34	720	83	293 K	[178]
PANi/graphene	In situ polymerization	46	394	82	293 K	[179]
PANI/graphene	In situ polymerization	26	814	55	–	[180]
PEDOT:PSS/rGO (21 wt%)	mixing	22.9	715.03	32.4	300k	[181]
Polyaniline (PANI)/GNs (30 wt %), HCl	In situ chemical polymerization	26	38	2.6	453 K	[182]

Based on the stated information of electrical conductivity and *S* regarding PANi/graphene-PEDOT: PSS/PANi/DWNT-PEDOT: PSS film, it is quite clear that it exhibits an exceptional power factor value i.e. reported as 2710 $\mu Wm^{-1}K^{-2}$. This considerable value surpasses all values reported for other OTEs at ambient temperatures, providing a great opportunity to utilize the waste heat at room temperatures in an eco-friendly way.

The weight ratio between components had a direct impact on the TE characteristics of multicomponent films. Liang et al. produced multi-component thin films made of PEDOT-tosylate (Tos)/SWCNTs/Te whose characteristics were strongly influenced by the SWCNTs' dispersion and the component's weight ratio. Initially, binary PEDOT-Tos/Te was

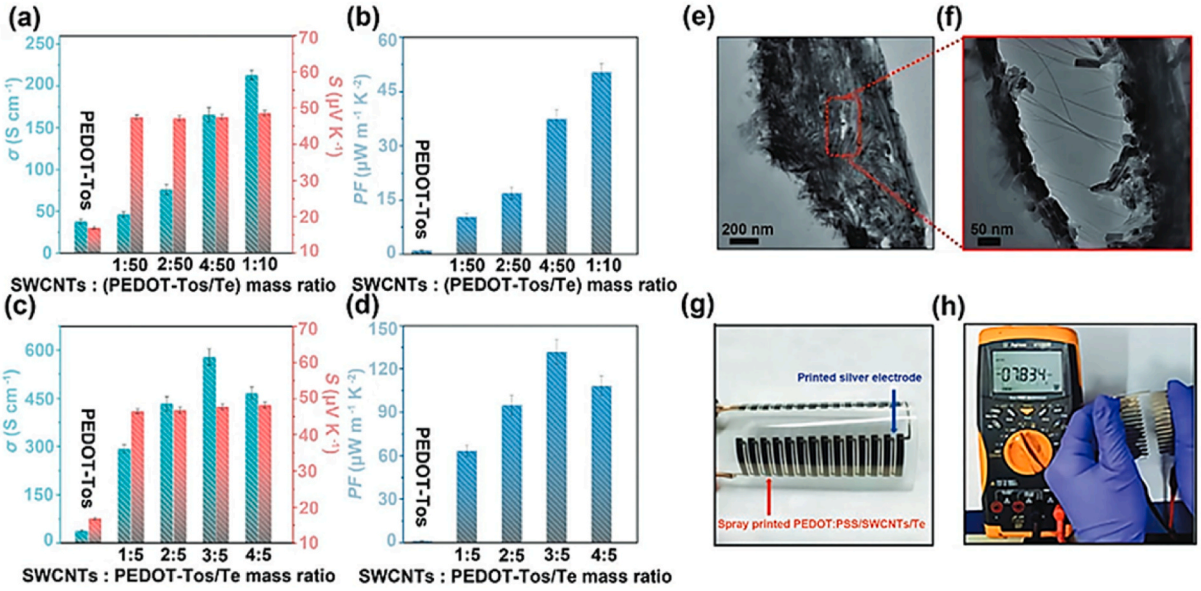

Fig. 11. (a,c) Ternary composites' conductivity and Seebeck coefficient when SWCNTs and pure PEDOT-Tos components are mixed in various bulk ratios. (b,d) PFs of related samples from various samples [186]. Copyright 2021, Wiley-VCH. (e,f) TEM cross-section illustration of PEDOT: PSS/SWCNTs/Te with a magnified view of the cracked region. g) Illustration of a bendable TEG. h) Photograph of a TE array with both sides kept at normal temperature producing voltage [187]. Copyright 2017, Royal Society of Chemistry.

created with various composition ratios to investigate the appropriate PEDOT-Tos content. The best PF value for the binary material could be obtained when the PEDOT-Tos concentration was 20 wt%. By mixing with SWCNTs at this ratio, the ideal TE properties of the ternary nanocomposite films were further studied. The electrical conductivity of multi-component material dramatically increased with an increase in SWCNT concentration, but the Seebeck coefficient essentially remained consistent (Fig. 11a–c) [186]. The highest *PF* was attained when the mass ratio of SWCNTs to PEDOT-Tos/Te was 3:5, which was 120 times greater w.r.t pristine PEDOT-Tos (Fig. 11b–d) [187].

Li et al. prepared a ternary composite i.e., poly(3,4-ethylenedioxythiophene)/graphene/CNT, by using physical mixing and in situ polymerization technologies, and the fabricated compound exhibited improved TE performance [188]. After this, a comparison of TE performances of the corresponding H_2SO_4 treated and untreated samples was made. The PEDOT/rGO/SWCNT-based ternary composites demonstrated maximum σ values compared to neat PEDOT, PEDOT/rGO binary composites. This increment is credited to the electrically integrated network, PEDOT molecules alignment, and molecular conformation transition. The acid-treated samples resulted in substantially high electrical conductivity, due to the reduction of neutral PSSH molecules. Both the acid treatment and ternary structure, simultaneously caused a significant influence on the *S* value. Increasing the CNT content leads to a rise in the *PF* value of ternary composites, resulting from a notable rise in electrical conductivity. However, PEDOT/rGO/SWCNT post-treated ternary composite, having a 10 wt% CNT, demonstrated four times greater *PF,* i.e., 9.1 $\mu Wm^{-1}K^{-2}$ compared to the untreated sample.

4.3.1. MXenes

In recent exploration of novel materials for thermoelectric applications, MXenes have received substantial attention owing to their excellent electrical conductivity and tunable surface chemistry. MXene are 2D transition metal carbides/nitrides having chemical formula as $M_{n+1}X_nT_x$ (n = 1–3, M denotes early transition metal (Sc, Zr, Hf, Mo, etc), A denotes elements of group 13 and 14, X represents carbon/nitrogen, and T_x shows surface terminations (OH/O/F). MXenes are obtained by the exfoliating of 'A' from the layered MAX phase materials exhibiting metallic properties with the general formula $M_{n+1}AX_n$. Exfoliation is enabled via M-A bonds, which have higher chemical activity than the stronger M-X bonds [189]. MXenes exhibit exceptional features rendering them suitable for thermoelectric (TE) applications such as hydrophilicity, flexible surface termination groups offering modifications and layered structure permits for suitable property regulation. Moreover, the transition metal atoms existing on the surface offer excessive redox activity, which is desirable for constructing thermo-electrochemical cells [190]. Since, MXene-based synthesized materials comprising pristine MXene, and nanocomposites MXene/-carbon, MXene/polymer composite, MXene/inorganic as well as fixed layers of a nano laminated structure with diverse molecule/ion intercalation [189–192] have applications in energy conversion, storage, and sensors technology [193–197]. However, considering the direction of this study, the doping of MXene with organic thermoelectric materials, and its impact on thermoelectric performance is highlighted.

The DFT and experimental investigations have anticipated that semiconducting MXenes exhibit a large Seebeck coefficient and higher electrical conductivity. Alternatively, polymer-based TE materials, PEDOT is considered as a potential material due to its ease of doping and high electrical conductivity. Therefore, doping the PEDOT with MXene is likely to enhance solution mixing, electrical conductivity, and increased stability [189–192,198]. There is only research on MAXene/PEDOT-based thermoelectrics. Guan et al. experimentally prepared MXene/PEDOT: PSS composite using drop casting a PEDOT: PSS and $Ti_3C_2T_x$ solution in water and DMSO. $Ti_3C_2T_x$ is known to be an n-type semiconductor, while PEDOT: PSS is a p-type. The electrons in $Ti_3C_2T_x$ can easily be converted to PEDOT: PSS by combining two such materials in a single fraction. As a result, an improved power factor (PF) of 155 $\mu Wm^{-1}k^{-2}$ is attained under the influence of the internal electric field stimulated by the unique p–n heterostructure. Most profoundly, the Seebeck coefficient (*S*) of nanocomposites reached 23 to 57.3 μVK^{-1} facilitated by the interfacial influence and the low-energy carriers' energy filtration [189–192,199]. Hence these results infer that the thermoelectric performance of PEDOT can be considerably improved by the formation of composites with MXene.

5. Thermoelectric generator applications

There are numerous uses for TEGs. Body heat, radioactive decay, waste heat, steel foundries, candles, gas flares, wood stoves, electronics, hot water pipes, solar photovoltaic panels, renewable energy sources, solar thermal, geothermal, combustion, any fuel source, external or internal combustion are heat sources that are frequently used with TEGs.

Battery, an exhaustible energy source, is mostly used to power such devices, which limits their lifetime and thus demands replacement after each finite time interval [200]. However, to reduce this limitation, several micro-energy harvesters have been developed [201], including piezoelectric devices, TPVs (Thermo-photovoltaic), TEGs (Thermo--electric Generators) and Triboelectric Generators etc. These harvesters perform the job of converting environmental energy, i.e., sunlight, human body heat, mechanical vibrations, etc., into electricity, thus causing a prolonged lifespan of biomedical devices along with the maintenance of a green-energy environment. TEGs, among all of these energy harvesters, are grabbing more attention because of their promising features, including higher durability and reliability at lower costs, minimum maintenance requirements, direct energy conversion without any intermediate mode, and eco-friendliness [202–205].

When it came to maintaining patient and medical device temperatures in the past, TEDs were widely used since dependability and noiseless operation were more crucial than COP. TEDs are gradually replacing devices that formerly relied on refrigeration cooling via a vapor compression cycle. The Medical Internet of Things (MioT) and next-generation wearable technology have made TEGs the industry's top tiny energy harvesters [206]. TEGs are a crucial component of an increasing number of implanted devices. Fig. 12a shows TEG inserted in human tissues under three layers, and a few implanted devices are shown in Fig. 12b. Since TEGs generate electricity through temperature differential, the human body must have a significant temperature gradient. TEGs should be put in the area of the body with the high-temperature variation to maximize their ability to produce electricity. When the body's internal temperature stays constant at 37 °C, where heat is vented into the environment, a high-temperature gradient is visible on the skin's surface [207].

In the fields of portable refrigeration and small-volume refrigeration, TE refrigerators are fiercely competitive [208]. Small-volume cooling applications are suited for TE refrigerators, and fine temperature control is possible by varying voltage or current. The advantages of TE refrigerators include their lack of a compressor, lack of mechanical moving parts, excellent dependability, lack of noise, and lack of need for refrigerant media like ammonia and Freon, which is more in line with contemporary society's demands for environmental protection [209]. Portable TE refrigerators, tiny TE air conditioners, TE air-conditioning seats, TE wine coolers, and TE water dispensers are some of the most popular applications as ordinary consumer items. Other applications include low-power Internet of Things (IoT) and wireless sensor networks (WSN) for environmental monitoring, as well as body heat-powered wrist clocks, flashlights, and medical sensors [210].

In the disciplines of optoelectronics and electronics, TE refrigerators are also extensively employed in devices like infrared detectors, laser diodes, photomultiplier tubes, CCD cameras, dew point testers, thermostatic baths, dehumidifiers, and freezing point osmometers (MEMs) [211]. Existing electronic devices can be categorized into four types based on their power consumption: high power (≥10 W), medium power

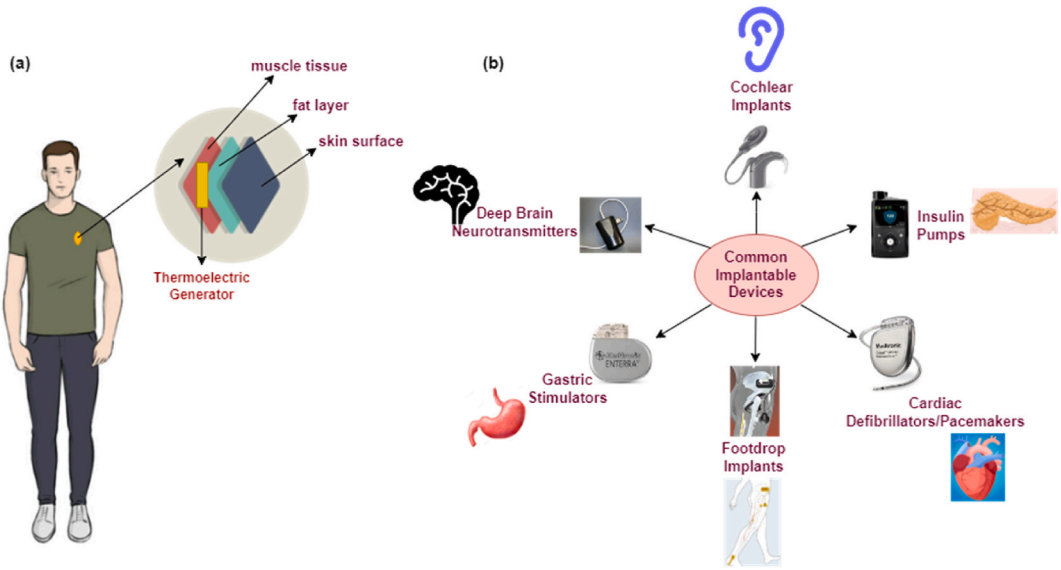

Fig. 12. (a) TEG inserted in human tissues under three layers (b) Typical implantable devices.

(1–10 W), low power (1 mW – 1W), and ultra-low power (≤1 mW). Due to the low-temperature differential in wearable and IoT systems, OTE devices are expected to be appropriate for ultra-low power consumption (≤1 mW) and self-powered devices. Existing studies on OTE devices primarily focus on achieving a higher zT value and reducing internal resistance in the TE leg to enhance thermal power output. Additionally, research studies aim to optimize the integration structure and density to increase the output voltage through logic circuit design. Furthermore, efforts are made to ensure that the device has a simpler fabrication process, good flexibility, and exceptional stretchability. Consequently, electronic sensors were developed that rely on OTEG and consist of thin-film organic TE legs placed on a paper substrate. These sensors are capable of producing an output voltage of 52.3 mV when placed on the skin, as shown in Fig. 13 (a) [212]. The paper-based OTEG, when combined with a sensing OFET that has extremely low power consumption, can effectively power a highly sensitive ammonia sensor for extended periods. This enables the development and use of Integrated Sensing Systems (ISSs). It is important to mention that the OTEG, known

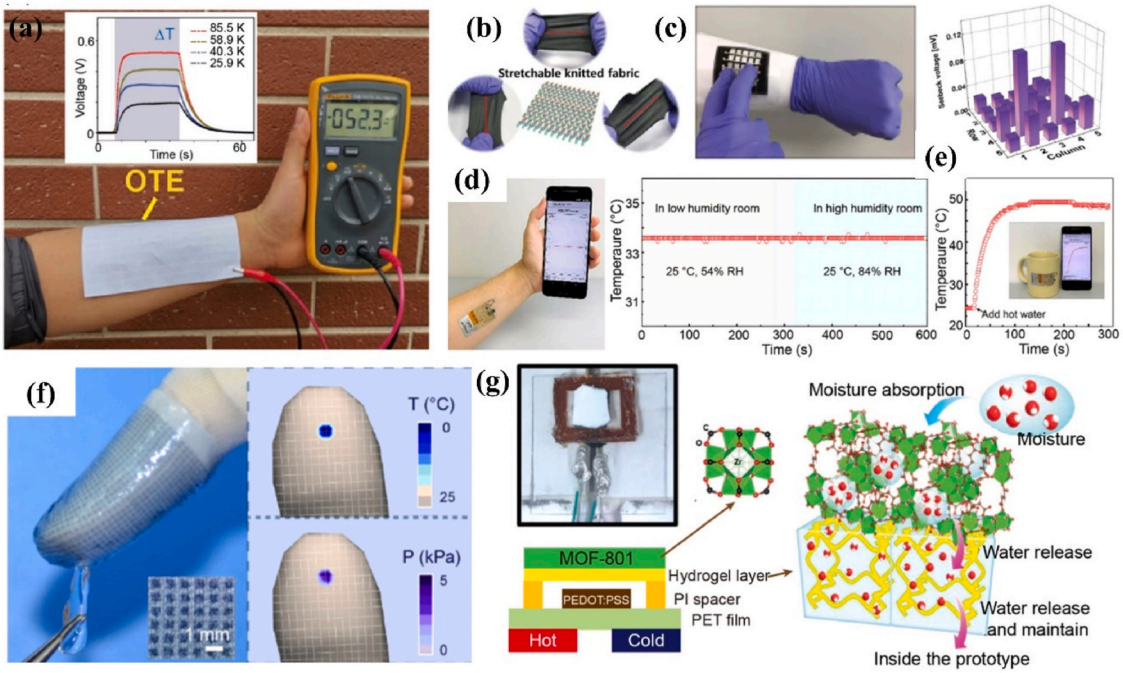

Fig. 13. (a) A photograph depicting an 18 × 9 OTE array attached to a human arm. The provided data represents the open-circuit voltage of the OTE array at various temperature differences (ΔT). Image of a multiaxis [212] (b) stretchable knitted fabric and (c) a wearable 5 × 5 sensor array with an analogous mapping of the output Seebeck voltage. Copyright 2018, The Royal Society of Chemistry (d) Schematic diagram and real-time temperature monitoring of a wireless sensor platform that is placed on an arm in various environmental humidity conditions [213] (e) Monitoring the temperature of a wireless sensing platform attached to a coffee cup after pouring hot water. P3HT refers to poly(3-hexylthiophene), whereas SEM stands for scanning electron microscope. (f) This is a photograph and a representation of the temperature and pressure distribution of a printed electronic finger touching an ice cube. The inset displays the optical microscope image of the MFSOTE matrix. The scale bar measures 1 mm. (g) The self-humidifying TE prototype consists of a MOF-801, a polymer hydrogel layer, a PI spacer, and a PET substrate. It is depicted in both a photograph and a schematic diagram. The right graph illustrates the process of absorbing, releasing, and maintaining moisture [214].

for its exceptional endurance and biocompatibility, is gaining more and more attention in the field of future smart electronics.

OTE materials and devices serve as efficient power sources in an individual or combined system, facilitating self-powered operation based on variations in external temperature. The OTE-based temperature sensor is the most prominent type of self-powered application, relying on the mechanism of thermoelectric generators. These devices generate the output voltage based on the temperature difference within the device ($\Delta T = \Delta V/S$). This voltage can be used to measure the real-time temperature when one electrode end is kept at a fixed temperature. Fig. 13 (b) illustrates the fabrication of a self-powered temperature sensor by Wang et al. [215]. The sensor is based on a composite of Te-nanowire and P3HT. The composites exhibited an increased Seebeck coefficient, resulting in a linear correlation between the output voltage and temperature at both ends of the devices. Therefore, the skin-attached OTEG may detect and response to a cooler that is in direct contact with the outside surface of the generator, resulting in a corresponding change in the output current signal. Composites consistently demonstrate useful characteristics when compared to pure OTE materials. Jeon & Bae et al. used a ternary compound ink that contains PEDOT: PSS, Ag nanoparticles, and graphene to fabricate a textile-based self-powered sensor that is both highly flexible and wearable. This sensor is illustrated in Fig. 13 (c) [216] The carefully designed, precisely layered p-n leg structure enhances the accuracy of temperature monitoring due to the direct contact between the junction and the heat source, which generates TE voltage. Thus, the utilization of stencil printing with composite ink is suitable for the production of large-area sensor arrays, as depicted in Fig. 13 (d). Self-powered temperature mapping can be achieved with a wearable device. Wang and Tokito et al. [217] developed a temperature sensor with great stability by using a crosslinker, specifically (3-glycidyloxypropyl) trimethoxysilane, and CYTOP to protect against the effects of vapors. The resulting sensor demonstrated excellent performance. The cross-linked P3HT device demonstrated a consistently high sensitivity of $-0.77\ \%\ ^{\circ}C^{-1}$ within the temperature range of 25 °C–50 °C, while the humidity varied from 30 % RH to 80 % RH. The inclusion of smart chips allows for real-time monitoring of temperature fluctuations in the human body and environment, resulting in outstanding sensing properties (Fig. 13e). The intelligence of the MFSOTE array (Fig. 13 (f)) may be further showcased through its flexibility, high level of integration, and sensitivity. This array was created using inkjet printing. The 1350 pixels inside a 2×3 cm^2 area facilitated the measurement of pressure and the collection of temperature data in the wearable intelligent components of artificial robotics and healthcare items. This technique is subsequently expanded upon to enable dual-parameter and triple-parameter sensing. Ha et al. demonstrated the development of a flexible array that mimics skin by using a nanocomposite of MWCNT and polyaniline to coat polyurethane foam [214].

An innovative design has been devised by incorporating a MOF-801/hydrogel self-humidifying bilayer to protect the sensor. This design allows for the modulation of moisture absorption and water amount in the device by managing water release and maintenance (Fig. 13 (g)). Through this architecture, the sensor based on PEDOT: PSS can maintain a consistent relative humidity and output voltage (V_{OC}) for 72 h, regardless of the surrounding environmental conditions. The ionic TE materials play a significant role in the captivating exploration of multifunctional sensing and bioelectronic circuits owing to their ion transport characteristics. Additional research should be conducted to enhance the environmental sustainability of self-powered sensors in various environments.

6. Summary and prospects

TE generators are less efficient when compared to other energy conversion technologies. Despite the swift progress of OTE materials, further work from the scientific community will be required in the future for practical applications. More research should be focused on gaining additional insight into the doping processes associated with the synthesis of cutting-edge organic semi(conductors) and dopants for TE applications. That's why the review is being designed to enhance the attention of the research community.

It is necessary to address the low conductivity induced by inadequate doping efficiency for n-type materials. Future research on OTEs should continue to focus on several other factors besides doping and materials composites that can enhance performance. CNT-enabled composites open up new avenues for engineering key interfaces to achieve superior performance. The molecular architecture and the detailed morphology of organic semiconductors, particularly in their pure forms or when combined with elements like carbon nanotubes (CNTs), are crucial yet complex to regulate and comprehensively understand. For instance, conducting thorough research on the vital functions of the conjugated backbone, lateral chains, and the correlation between the polymer's molecular weight and its thermoelectric efficiency is essential. Such studies can provide valuable insights for selecting materials in future developments. As more studies delve into the intriguing area of TE materials, there is reason to believe that TE $zT > 1$ will skyrocket during the next decade. Enhanced energy production from materials will inevitably lead to extensive use in garments and mobile gadgets with charging capabilities using body heat.

Technically, accurate measurements of critical thermoelectric properties for organic thermoelectric materials, which are usually developed as thin polymer films, differ from inorganic bulk materials. The Seebeck coefficients and in-plane thermal conductivities published by multiple groups have been determined using various homemade systems, among which are influenced by environmental conditions, sample size, shape, and substrate. Thus, the consequent precision and consistency must be addressed. Due to the diversity of structures and types of organic thermoelectric devices, there is no standard for testing their performance. More research in this area will surely be beneficial to the continued advancement and development of high-performance thermoelectric devices.

Additionally, the integration of unconventional materials, such as crystalline frameworks and porous structures, represents an untapped frontier with promising potential for groundbreaking advancements in thermoelectric materials and devices. This approach not only addresses extant gaps in the field but also sets the stage for revolutionary breakthroughs, ushering in a new era of efficient and versatile thermoelectric technologies.

The wearable and demotic industries have a lot of potential for OTEG applications because they function well at temperatures near ambient temperature. The eventual viability of OTEG in the market will be possible only if efficient processing techniques for big-area industries are used and integrated in such a way that competitive TE efficiencies are maintained in everyday use.

CRediT authorship contribution statement

Misbah Sehar Abbasi: Conceptualization, Data curation, Formal analysis, Writing – original draft. **Rabia Sultana:** Data curation, Formal analysis, Visualization, Writing – original draft. **Iftikhar Ahmed:** Visualization. **Muhammad Adnan:** Data curation, Visualization. **Usman Ali Shah:** Data curation, Validation. **Muhammad Sultan Irshad:** Conceptualization, Project administration, Supervision, Writing – original draft, Writing – review & editing. **Hung Ngoc Vu:** Data curation, Visualization. **Lien Thi Do:** Validation. **Hong Ha Thi Vu:** Data curation, Formal analysis, Validation. **Thuy-Duong Pham:** Formal analysis, Validation. **Ho Xuan Nang:** Formal analysis, Validation, Visualization. **Van-Duong Dao:** Conceptualization, Funding acquisition, Investigation, Project administration, Supervision, Writing – original draft, Writing – review & editing.

Declaration of competing interest

The authors declare that they have no known competing financial interests or personal relationships that could have appeared to influence the work reported in this paper.

Data availability

Data will be made available on request.

Acknowledgments

We acknowledge the financial support from the Vietnam National Foundation for Science and Technology Development (NAFOSTED) under grant number 103.02–2021.106 and Phenikaa Innovation Foundation grant (ĐMST.2022.02).The authors extend their appreciation to Abu Dhabi University for funding this work through Mubadala-Abu Dhabi University Collaborative Projects Awards-2nd cycle AY23/24.

References

[1] Smith C, Hill AK, Torrente-Murciano L. Current and future role of Haber–Bosch ammonia in a carbon-free energy landscape. Energy Environ Sci 2020;13:331–44. https://doi.org/10.1039/C9EE02873K.
[2] Poizot P, Dolhem F. Clean energy new deal for a sustainable world: from non-CO2 generating energy sources to greener electrochemical storage devices. Energy Environ Sci 2011;4:2003. https://doi.org/10.1039/c0ee00731e.
[3] Ahmadi S, Raeisi M, Eslami L, Rajabpour A. Thermoelectric characteristics of two-dimensional structures for three different lattice compounds of B-C-N and graphene counterpart BX (X = P, as, and Sb) systems. J Phys Chem C 2021;125. https://doi.org/10.1021/acs.jpcc.1c03460.
[4] Kim CS, Yang HM, Lee J, Lee GS, Choi H, Kim YJ, et al. Self-powered wearable electrocardiography using a wearable thermoelectric power generator. ACS Energy Lett 2018;3. https://doi.org/10.1021/acsenergylett.7b01237.
[5] Cheng H, Du Y, Wang B, Mao Z, Xu H, Zhang L, et al. Flexible cellulose-based thermoelectric sponge towards wearable pressure sensor and energy harvesting. Chem Eng J 2018;338:1–7. https://doi.org/10.1016/j.cej.2017.12.134.
[6] Kim CS, Yang HM, Lee J, Lee GS, Choi H, Kim YJ, et al. Self-powered wearable electrocardiography using a wearable thermoelectric power generator. ACS Energy Lett 2018;3:501–7. https://doi.org/10.1021/acsenergylett.7b01237.
[7] Zhou M, Al-Furjan MSH, Zou J, Liu W. A review on heat and mechanical energy harvesting from human – principles, prototypes and perspectives. Renew Sustain Energy Rev 2018;82:3582–609. https://doi.org/10.1016/j.rser.2017.10.102.
[8] Cheng H, Du Y, Wang B, Mao Z, Xu H, Zhang L, et al. Flexible cellulose-based thermoelectric sponge towards wearable pressure sensor and energy harvesting. Chem Eng J 2018;338:1–7. https://doi.org/10.1016/j.cej.2017.12.134.
[9] Zhang D, Wang Y, Yang Y. Design, performance, and application of thermoelectric nanogenerators. Small 2019;15:1805241. https://doi.org/10.1002/smll.201805241.
[10] Ouyang Z, Li D. Modelling of segmented high-performance thermoelectric generators with effects of thermal radiation, electrical and thermal contact resistances. Sci Rep 2016;6:24123. https://doi.org/10.1038/srep24123.
[11] Du Y, Xu J, Paul B, Eklund P. Flexible thermoelectric materials and devices. Appl Mater Today 2018;12:366–88. https://doi.org/10.1016/j.apmt.2018.07.004.
[12] Fiedler C, Kleinhanns T, Garcia M, Lee S, Calcabrini M, Ibáñez M. Solution-processed inorganic thermoelectric materials: opportunities and challenges. Chem Mater 2022;34:8471–89. https://doi.org/10.1021/acs.chemmater.2c01967.
[13] Xu X, Zhao Y, Liu Y. Wearable electronics based on stretchable organic semiconductors. Small 2023:2206309. https://doi.org/10.1002/smll.202206309.
[14] Root SE, Savagatrup S, Printz AD, Rodriquez D, Lipomi DJ. Mechanical properties of organic semiconductors for stretchable, highly flexible, and mechanically robust electronics. Chem Rev 2017;117:6467–99. https://doi.org/10.1021/acs.chemrev.7b00003.
[15] Haddad C, Périlhon C, Danlos A, François M-X, Descombes G. Some efficient solutions to recover low and medium waste heat: competitiveness of the thermoacoustic technology. Energy Proc 2014;50:1056–69. https://doi.org/10.1016/j.egypro.2014.06.125.
[16] Soleimani Z, Zoras S, Ceranic B, Shahzad S, Cui Y. A review on recent developments of thermoelectric materials for room-temperature applications. Sustain Energy Technol Assessments 2020;37:100604. https://doi.org/10.1016/j.seta.2019.100604.
[17] Li J, Huckleby AB, Zhang M. Polymer-based thermoelectric materials: a review of power factor improving strategies. Journal of Materiomics 2022;8:204–20. https://doi.org/10.1016/j.jmat.2021.03.013.
[18] Beretta D, Perego A, Lanzani G, Caironi M. Organic flexible thermoelectric generators: from modeling, a roadmap towards applications. Sustain Energy Fuels 2017;1:174–90. https://doi.org/10.1039/C6SE00028B.
[19] Tripathi A, Lee Y, Lee S, Woo HY. Recent advances in n-type organic thermoelectric materials, dopants, and doping strategies. J Mater Chem C Mater 2022;10:6114–40. https://doi.org/10.1039/D1TC06175E.
[20] Ismael A, Al-Jobory A, Wang X, Alshehab A, Almutlg A, Alshammari M, et al. Molecular-scale thermoelectricity: as simple as 'ABC.'. Nanoscale Adv 2020;2:5329–34. https://doi.org/10.1039/D0NA00772B.
[21] Gemma A, Gotsmann B. A roadmap for molecular thermoelectricity. Nat Nanotechnol 2021;16:1299–301. https://doi.org/10.1038/s41565-021-01012-0.
[22] Park S, Kang S, Yoon HJ. Thermopower of molecular junction in harsh thermal environments. Nano Lett 2022;22:3953–60. https://doi.org/10.1021/acs.nanolett.2c00422.
[23] Tan A, Balachandran J, Sadat S, Gavini V, Dunietz BD, Jang S-Y, et al. Effect of length and contact chemistry on the electronic structure and thermoelectric properties of molecular junctions. J Am Chem Soc 2011;133:8838–41. https://doi.org/10.1021/ja202178k.
[24] Liu Z, Chen G. Advancing flexible thermoelectric devices with polymer composites. Adv Mater Technol 2020;5:2000049. https://doi.org/10.1002/admt.202000049.
[25] Kinloch IA, Suhr J, Lou J, Young RJ, Ajayan PM. Composites with carbon nanotubes and graphene: an outlook. Science 2018;362:547–53. https://doi.org/10.1126/science.aat7439.
[26] Thermoelectric materials and devices. Elsevier; 2021. https://doi.org/10.1016/C2018-0-02472-X.
[27] Van Herwaarden AW, Sarro PM. Thermal sensors based on the seebeck effect. Sensor Actuator 1986;10:321–46. https://doi.org/10.1016/0250-6874(86)80053-1.
[28] Terasaki I. Thermal conductivity and thermoelectric power of semiconductors. Comprehensive semiconductor science and technology. Elsevier; 2011. p. 326–58. https://doi.org/10.1016/B978-0-44-453153-7.00070-5.
[29] Zhang L, Shi X-L, Yang Y-L, Chen Z-G. Flexible thermoelectric materials and devices: from materials to applications. Mater Today 2021;46:62–108. https://doi.org/10.1016/j.mattod.2021.02.016.
[30] Snyder GJ, Toberer ES. Complex thermoelectric materials. Nat Mater 2008;7:105–14. https://doi.org/10.1038/nmat2090.
[31] Liu D, Shi P, Ren W, Liu Y, Niu G, Liu M, et al. A new kind of thermocouple made of p-type and n-type semi-conductive oxides with giant thermoelectric voltage for high temperature sensing. J Mater Chem C Mater 2018;6:3206–11. https://doi.org/10.1039/C8TC00171E.
[32] Tan G, Ohta M, Kanatzidis MG. Thermoelectric power generation: from new materials to devices. Phil Trans Math Phys Eng Sci 2019;377:20180450. https://doi.org/10.1098/rsta.2018.0450.
[33] Wei Q, Mukaida M, Kirihara K, Naitoh Y, Ishida T. Recent progress on PEDOT-based thermoelectric materials. Materials 2015;8:732–50. https://doi.org/10.3390/ma8020732.
[34] Jha PK. Strategies for improving efficiency of thermoelectric materials. Thermoelectricity and Advanced Thermoelectric Materials 2021:117–38. https://doi.org/10.1016/B978-0-12-819984-8.00003-5. Elsevier.
[35] Xie WJ, He J, Zhu S, Su XL, Wang SY, Holgate T, et al. Simultaneously optimizing the independent thermoelectric properties in (Ti,Zr,Hf)(Co,Ni)Sb alloy by in situ forming InSb nanoinclusions. Acta Mater 2010;58:4705–13. https://doi.org/10.1016/j.actamat.2010.05.005.
[36] Yadav A, Deshmukh P, Roberts K, Jisrawi N, Valluri S. An analytic study of the Wiedemann–Franz law and the thermoelectric figure of merit. J Phys Commun 2019;3:105001. https://doi.org/10.1088/2399-6528/ab444a.
[37] Gayner C, Amouyal Y. Energy filtering of charge carriers: current trends, challenges, and prospects for thermoelectric materials. Adv Funct Mater 2020;30:1901789. https://doi.org/10.1002/adfm.201901789.
[38] Blackburn JL, Ferguson AJ, Cho C, Grunlan JC. Thermoelectric materials: carbon-nanotube-based thermoelectric materials and devices (adv. Mater. 11/2018). Adv Mater 2018;30:1870072. https://doi.org/10.1002/adma.201870072.
[39] Firth A, Zhang B, Yang A. Quantification of global waste heat and its environmental effects. Appl Energy 2019;235:1314–34. https://doi.org/10.1016/j.apenergy.2018.10.102.
[40] Tang ZB, Deng YD, Su CQ, Shuai WW, Xie CJ. A research on thermoelectric generator's electrical performance under temperature mismatch conditions for automotive waste heat recovery system. Case Stud Therm Eng 2015;5:143–50. https://doi.org/10.1016/j.csite.2015.03.006.
[41] Ranjan M, Maiti T. Device modeling and performance optimization of thermoelectric generators under isothermal and isoflux heat source condition. J Power Sources 2020;480:228867. https://doi.org/10.1016/j.jpowsour.2020.228867.
[42] Tritt TM, Böttner H, Chen L. Thermoelectrics: direct solar thermal energy conversion. MRS Bull 2008;33:366–8. https://doi.org/10.1557/mrs2008.73.
[43] Vineis CJ, Shakouri A, Majumdar A, Kanatzidis MG. Nanostructured thermoelectrics: big efficiency gains from small features. Adv Mater 2010;22:3970–80. https://doi.org/10.1002/adma.201000839.
[44] Yan Q, Kanatzidis MG. High-performance thermoelectrics and challenges for practical devices. Nat Mater 2022;21:503–13. https://doi.org/10.1038/s41563-021-01109-w.
[45] Khalid K, Tan X, Mohd Zaid HF, Tao Y, Lye Chew C, Chu D-T, et al. Advanced in developmental organic and inorganic nanomaterial: a review. Bioengineered 2020;11:328–55. https://doi.org/10.1080/21655979.2020.1736240.
[46] Newnham JA, Zhao T, Gibson QD, Manning TD, Zanella M, Mariani E, et al. Band structure engineering of $Bi_4O_4SeCl_2$ for thermoelectric applications. ACS Organic & Inorganic Au 2022;2:405–14. https://doi.org/10.1021/acsorginorgau.2c00018.

[47] Méndez H, Heimel G, Opitz A, Sauer K, Barkowski P, Oehzelt M, et al. Doping of organic semiconductors: impact of dopant strength and electronic coupling. Angew Chem Int Ed 2013;52:7751–5. https://doi.org/10.1002/anie.201302396.
[48] Huseynova G, Lee J, Lee J-H, Lee J-H. Charge generation efficiency of electrically doped organic semiconductors. Mater Today Energy 2021;21:100709. https://doi.org/10.1016/j.mtener.2021.100709.
[49] Salzmann I, Heimel G, Oehzelt M, Winkler S, Koch N. Molecular electrical doping of organic semiconductors: fundamental mechanisms and emerging dopant design rules. Acc Chem Res 2016;49:370–8. https://doi.org/10.1021/acs.accounts.5b00438.
[50] Russ B, Glaudell A, Urban JJ, Chabinyc ML, Segalman RA. Organic thermoelectric materials for energy harvesting and temperature control. Nat Rev Mater 2016;1:16050. https://doi.org/10.1038/natrevmats.2016.50.
[51] Sirringhaus H. 25th anniversary article: organic field-effect transistors: the path beyond amorphous silicon. Adv Mater 2014;26:1319–35. https://doi.org/10.1002/adma.201304346.
[52] Dou L, You J, Hong Z, Xu Z, Li G, Street RA, et al. 25th anniversary article: a decade of organic/polymeric photovoltaic research. Adv Mater 2013;25:6642–71. https://doi.org/10.1002/adma.201302563.
[53] Fabretto MV, Evans DR, Mueller M, Zuber K, Hojati-Talemi P, Short RD, et al. Polymeric material with metal-like conductivity for next generation organic electronic devices. Chem Mater 2012;24:3998–4003. https://doi.org/10.1021/cm302899v.
[54] Heeger AJ. Semiconducting and metallic polymers: the fourth generation of polymeric materials. J Phys Chem B 2001;105:8475–91. https://doi.org/10.1021/jp011611w.
[55] Worfolk BJ, Andrews SC, Park S, Reinspach J, Liu N, Toney MF, et al. Ultrahigh electrical conductivity in solution-sheared polymeric transparent films. In: Proceedings of the national academy of sciences, vol. 112; 2015. p. 14138–43. https://doi.org/10.1073/pnas.1509958112.
[56] Wang S, Zuo G, Kim J, Sirringhaus H. Progress of conjugated polymers as emerging thermoelectric materials. Prog Polym Sci 2022;129:101548. https://doi.org/10.1016/j.progpolymsci.2022.101548.
[57] Nandihalli N, Liu C-J, Mori T. Polymer based thermoelectric nanocomposite materials and devices: fabrication and characteristics. Nano Energy 2020;78:105186. https://doi.org/10.1016/j.nanoen.2020.105186.
[58] Bharti M, Singh A, Samanta S, Aswal DK. Conductive polymers for thermoelectric power generation. Prog Mater Sci 2018;93:270–310. https://doi.org/10.1016/j.pmatsci.2017.09.004.
[59] Wang L, Jia X, Wang D, Zhu G, Li J. Preparation and thermoelectric properties of polythiophene/multiwalled carbon nanotube composites. Synth Met 2013;181:79–85. https://doi.org/10.1016/j.synthmet.2013.08.011.
[60] Advanced PEDOT thermoelectric materials. Elsevier; 2022. https://doi.org/10.1016/C2019-0-03613-8.
[61] Yassar A, Roncali J, Garnier F. Conductivity and conjugation length in poly(3-methylthiophene) thin films. Macromolecules 1989;22:804–9. https://doi.org/10.1021/ma00192a049.
[62] Sun Y-C, Terakita D, Tseng AC, Naguib HE. Study on the thermoelectric properties of PVDF/MWCNT and PVDF/GNP composite foam. Smart Mater Struct 2015;24:085034. https://doi.org/10.1088/0964-1726/24/8/085034.
[63] Masubuchi S, Imai R, Yamazaki K, Kazama S, Takada J, Matsuyama T. Structure and electrical transport property of poly(3-octylthiophene). Synth Met 1999;101:594–5. https://doi.org/10.1016/S0379-6779(98)01156-4.
[64] Lim E, Peterson KA, Su GM, Chabinyc ML. Thermoelectric properties of poly(3-hexylthiophene) (P3HT) doped with 2,3,5,6-Tetrafluoro-7,7,8,8-tetracyanoquinodimethane (F_4 TCNQ) by vapor-phase infiltration. Chem Mater 2018;30:998–1010. https://doi.org/10.1021/acs.chemmater.7b04849.
[65] Wang D, Liu L, Gao X, Di C, Zhu D. Recent advances in molecular design of organic thermoelectric materials. CCS Chem 2021;3:2212–25. https://doi.org/10.31635/ccschem.021.202101076.
[66] Yue R, Xu J. Poly(3,4-ethylenedioxythiophene) as promising organic thermoelectric materials: a mini-review. Synth Met 2012;162:912–7. https://doi.org/10.1016/j.synthmet.2012.04.005.
[67] Du Y, Shen SZ, Cai K, Casey PS. Research progress on polymer–inorganic thermoelectric nanocomposite materials. Prog Polym Sci 2012;37:820–41. https://doi.org/10.1016/j.progpolymsci.2011.11.003.
[68] Wei Q, Mukaida M, Kirihara K, Naitoh Y, Ishida T. Recent progress on PEDOT-based thermoelectric materials. Materials 2015;8:732–50. https://doi.org/10.3390/ma8020732.
[69] Wen N, Fan Z, Yang S, Zhao Y, Cong T, Xu S, et al. Highly conductive, ultra-flexible and continuously processable PEDOT:PSS fibers with high thermoelectric properties for wearable energy harvesting. Nano Energy 2020;78:105361. https://doi.org/10.1016/j.nanoen.2020.105361.
[70] Xia Y, Sun K, Ouyang J. Solution-processed metallic conducting polymer films as transparent electrode of optoelectronic devices. Adv Mater 2012;24:2436–40. https://doi.org/10.1002/adma.201104795.
[71] Kim N, Kee S, Lee SH, Lee BH, Kahng YH, Jo Y-R, et al. Highly conductive PEDOT:PSS nanofibrils induced by solution-processed crystallization. Adv Mater 2014;26:2268–72. https://doi.org/10.1002/adma.201304611.
[72] Liu G, Liu Y, Zhang M, Yang Z, Gane P. Comparing build architecture and electrolyte of ITO-free flexible patterned organic screen-printed ECDs based on a novel PEDOT:PSS compound film post-treated with strong and weak organic acids. Org Electron 2020;81:105674. https://doi.org/10.1016/j.orgel.2020.105674.
[73] Kirihara K, Wei Q, Mukaida M, Ishida T. Reduction of specific contact resistance between the conducting polymer PEDOT:PSS and a metal electrode by addition of a second solvent during film formation and a post-surface treatment. Synth Met 2018;246:289–96. https://doi.org/10.1016/j.synthmet.2018.11.005.
[74] Liu C, Lu B, Yan J, Xu J, Yue R, Zhu Z, et al. Highly conducting free-standing poly(3,4-ethylenedioxythiophene)/poly(styrenesulfonate) films with improved thermoelectric performances. Synth Met 2010;160:2481–5. https://doi.org/10.1016/j.synthmet.2010.09.031.
[75] Saxena N, Pretzl B, Lamprecht X, Bießmann L, Yang D, Li N, et al. Ionic liquids as post-treatment agents for simultaneous improvement of seebeck coefficient and electrical conductivity in PEDOT:PSS films. ACS Appl Mater Interfaces 2019;11:8060–71. https://doi.org/10.1021/acsami.8b21709.
[76] Yemata TA, Zheng Y, Kyaw AKK, Wang X, Song J, Chin WS, et al. Improved thermoelectric properties and environmental stability of conducting PEDOT:PSS films post-treated with imidazolium ionic liquids. Front Chem 2020;7. https://doi.org/10.3389/fchem.2019.00870.
[77] Li J, Tang X, Li H, Yan Y, Zhang Q. Synthesis and thermoelectric properties of hydrochloric acid-doped polyaniline. Synth Met 2010;160:1153–8. https://doi.org/10.1016/j.synthmet.2010.03.001.
[78] Liu J, Jia Y, Jiang Q, Jiang F, Li C, Wang X, et al. Highly conductive hydrogel polymer fibers toward promising wearable thermoelectric energy harvesting. ACS Appl Mater Interfaces 2018;10:44033–40. https://doi.org/10.1021/acsami.8b15332.
[79] Jangra V, Maity S, Vishnoi P. A review on the development of conjugated polymer-based textile thermoelectric generator. J Ind Textil 2022;51:181S–214S. https://doi.org/10.1177/1528083721996732.
[80] Chiang J-C, MacDiarmid AG. 'Polyaniline': protonic acid doping of the emeraldine form to the metallic regime. Synth Met 1986;13:193–205. https://doi.org/10.1016/0379-6779(86)90070-6.
[81] Yoon CO, Reghu M, Moses D, Heeger AJ, Cao Y, Chen T-A, et al. Hopping transport in doped conducting polymers in the insulating regime near the metal-insulator boundary: polypyrrole, polyaniline and polyalkylthiophenes. Synth Met 1995;75:229–39. https://doi.org/10.1016/0379-6779(96)80013-0.
[82] Yao Q, Wang Q, Wang L, Wang Y, Sun J, Zeng H, et al. The synergic regulation of conductivity and Seebeck coefficient in pure polyaniline by chemically changing the ordered degree of molecular chains. J Mater Chem A 2014;2:2634–40. https://doi.org/10.1039/C3TA14008C.
[83] Wang H, Yin L, Pu X, Yu C. Facile charge carrier adjustment for improving thermopower of doped polyaniline. Polymer 2013;54:1136–40. https://doi.org/10.1016/j.polymer.2012.12.038.
[84] Nath C, Kumar A. Fractal like charge transport in polyaniline nanostructures. Phys B Condens Matter 2013;426:94–102. https://doi.org/10.1016/j.physb.2013.06.019.
[85] Li H, Liang Y, Liu S, Qiao F, Li P, He C. Modulating carrier transport for the enhanced thermoelectric performance of carbon nanotubes/polyaniline composites. Org Electron 2019;69:62–8. https://doi.org/10.1016/j.orgel.2019.03.006.
[86] Li H, Liu S, Li P, Yuan D, Zhou X, Sun J, et al. Interfacial control and carrier tuning of carbon nanotube/polyaniline composites for high thermoelectric performance. Carbon N Y 2018;136:292–8. https://doi.org/10.1016/j.carbon.2018.04.083.
[87] Toshima N, Imai M, Ichikawa S. Organic–inorganic nanohybrids as novel thermoelectric materials: hybrids of polyaniline and bismuth(III) telluride nanoparticles. J Electron Mater 2011;40:898–902. https://doi.org/10.1007/s11664-010-1403-1.
[88] Kang YH, Ko S-J, Lee M-H, Lee YK, Kim BJ, Cho SY. Highly efficient and air stable thermoelectric devices of poly(3-hexylthiophene) by dual doping of Au metal precursors. Nano Energy 2021;82:105681. https://doi.org/10.1016/j.nanoen.2020.105681.
[89] Gregory SA, Menon AK, Ye S, Seferos DS, Reynolds JR, Yee SK. Effect of heteroatom and doping on the thermoelectric properties of poly(3-alkylchalcogenophenes). Adv Energy Mater 2018;8:1802419. https://doi.org/10.1002/aenm.201802419.
[90] Russ B, Robb MJ, Brunetti FG, Miller PL, Perry EE, Patel SN, et al. Power factor enhancement in solution-processed organic n-type thermoelectrics through molecular design. Adv Mater 2014;26:3473–7. https://doi.org/10.1002/adma.201306116.
[91] Schlitz RA, Brunetti FG, Glaudell AM, Miller PL, Brady MA, Takacs CJ, et al. Solubility-limited extrinsic n-type doping of a high electron mobility polymer for thermoelectric applications. Adv Mater 2014;26:2825–30. https://doi.org/10.1002/adma.201304866.
[92] Piliego C, Jarzab D, Gigli G, Chen Z, Facchetti A, Loi MA. High electron mobility and ambient stability in solution-processed perylene-based organic field-effect transistors. Adv Mater 2009;21:1573–6. https://doi.org/10.1002/adma.200803207.
[93] Kiefer D, Giovannitti A, Sun H, Biskup T, Hofmann A, Koopmans M, et al. Enhanced n-doping efficiency of a naphthalenediimide-based copolymer through polar side chains for organic thermoelectrics. ACS Energy Lett 2018;3:278–85. https://doi.org/10.1021/acsenergylett.7b01146.
[94] Nava D, Shin Y, Massetti M, Jiao X, Biskup T, Jagadeesh MS, et al. Drastic improvement of air stability in an n-type doped naphthalene-diimide polymer by thionation. ACS Appl Energy Mater 2018;1:4626–34. https://doi.org/10.1021/acsaem.8b00777.
[95] Russ B, Robb MJ, Popere BC, Perry EE, Mai C-K, Fronk SL, et al. Tethered tertiary amines as solid-state n-type dopants for solution-processable organic semiconductors. Chem Sci 2016;7:1914–9. https://doi.org/10.1039/C5SC04217H.
[96] Kiefer D, Giovannitti A, Sun H, Biskup T, Hofmann A, Koopmans M, et al. Enhanced n-doping efficiency of a naphthalenediimide-based copolymer through

polar side chains for organic thermoelectrics. ACS Energy Lett 2018;3:278–85. https://doi.org/10.1021/acsenergylett.7b01146.
[97] Schlitz RA, Brunetti FG, Glaudell AM, Miller PL, Brady MA, Takacs CJ, et al. Solubility-limited extrinsic n-type doping of a high electron mobility polymer for thermoelectric applications. Adv Mater 2014;26:2825–30. https://doi.org/10.1002/adma.201304866.
[98] Qiu L, Liu J, Alessandri R, Qiu X, Koopmans M, Havenith RWA, et al. Enhancing doping efficiency by improving host-dopant miscibility for fullerene-based n-type thermoelectrics. J Mater Chem A 2017;5:21234–41. https://doi.org/10.1039/C7TA06609K.
[99] Wang L, Liu F, Jin C, Zhang T, Yin Q. Preparation of polypyrrole/graphene nanosheets composites with enhanced thermoelectric properties. RSC Adv 2014;4:46187–93. https://doi.org/10.1039/C4RA07774A.
[100] Huang D, Yao H, Cui Y, Zou Y, Zhang F, Wang C, et al. Conjugated-backbone effect of organic small molecules for n-type thermoelectric materials with ZT over 0.2. J Am Chem Soc 2017;139:13013–23. https://doi.org/10.1021/jacs.7b05344.
[101] Barbot A, Di Bin C, Lucas B, Ratier B, Aldissi M. N-type doping and thermoelectric properties of co-sublimed cesium-carbonate-doped fullerene. J Mater Sci 2013;48:2785–9. https://doi.org/10.1007/s10853-012-6824-1.
[102] Slack G. New materials and performance limits for thermoelectric cooling. CRC Handbook of Thermoelectrics 1995. https://doi.org/10.1201/9781420049718.ch34. CRC Press.
[103] Beekman M, Morelli DT, Nolas GS. Better thermoelectrics through glass-like crystals. Nat Mater 2015;14:1182–5. https://doi.org/10.1038/nmat4461.
[104] Liu J, Ye G, Zee B van der, Dong J, Qiu X, Liu Y, et al. N-type organic thermoelectrics of donor-acceptor copolymers: improved power factor by molecular tailoring of the density of states. Adv Mater 2018;30:1804290. https://doi.org/10.1002/adma.201804290.
[105] Zuo G, Li Z, Wang E, Kemerink M. High seebeck coefficient and power factor in n-type organic thermoelectrics. Adv Electron Mater 2018;4:1700501. https://doi.org/10.1002/aelm.201700501.
[106] Yang C-Y, Stoeckel M-A, Ruoko T-P, Wu H-Y, Liu X, Kolhe NB, et al. A high-conductivity n-type polymeric ink for printed electronics. Nat Commun 2021;12:2354. https://doi.org/10.1038/s41467-021-22528-y.
[107] Xuan Y, Liu X, Desbief S, Leclère P, Fahlman M, Lazzaroni R, et al. Thermoelectric properties of conducting polymers: the case of poly(3-hexylthiophene). Phys Rev B 2010;82:115454. https://doi.org/10.1103/PhysRevB.82.115454.
[108] Kaiser AB. Systematic conductivity behavior in conducting polymers: effects of heterogeneous disorder. Adv Mater 2001;13:927–41. https://doi.org/10.1002/1521-4095(200107)13:12/13<927::AID-ADMA927>3.0.CO;2-B.
[109] Gao X, Uehara K, Klug DD, Patchkovskii S, Tse JS, Tritt TM. Theoretical studies on the thermopower of semiconductors and low-band-gap crystalline polymers. Phys Rev B 2005;72:125202. https://doi.org/10.1103/PhysRevB.72.125202.
[110] Kiess HG, editor. Conjugated conducting polymers, vol. 102. Berlin, Heidelberg: Springer Berlin Heidelberg; 1992. https://doi.org/10.1007/978-3-642-46729-5.
[111] Kaiser AB. Thermoelectric power and conductivity of heterogeneous conducting polymers. Phys Rev B 1989;40:2806–13. https://doi.org/10.1103/PhysRevB.40.2806.
[112] Feng-Xing J, Jing-Kun X, Bao-Yang L, Yu X, Rong-Jin H, Lai-Feng L. Thermoelectric performance of poly(3,4-ethylenedioxythiophene): poly (styrenesulfonate). Chin Phys Lett 2008;25:2202–5. https://doi.org/10.1088/0256-307X/25/6/076.
[113] Haneef HF, Zeidell AM, Jurchescu OD. Charge carrier traps in organic semiconductors: a review on the underlying physics and impact on electronic devices. J Mater Chem C Mater 2020;8:759–87. https://doi.org/10.1039/C9TC05695E.
[114] Lee TS, Nam S, Oh JG, Suh EH, Jung J, Oh H, et al. Highly surface-conformable thermoelectric patches for efficient thermal contact with arbitrary substrates. Chem Eng J 2023;455:140925. https://doi.org/10.1016/j.cej.2022.140925.
[115] Melnikov P, Bobrov A, Marfin Y. On the use of polymer-based composites for the creation of optical sensors: a review. Polymers 2022;14:4448. https://doi.org/10.3390/polym14204448.
[116] Allard S, Forster M, Souharce B, Thiem H, Scherf U. Organic semiconductors for solution-processable field-effect transistors (OFETs). Angew Chem Int Ed 2008;47:4070–98. https://doi.org/10.1002/anie.200701920.
[117] Ahmad S. Organic semiconductors for device applications: current trends and future prospects. J Polym Eng 2014;34:279–338. https://doi.org/10.1515/polyeng-2013-0267.
[118] Zhang Y, Heo Y-J, Park M, Park S-J. Recent advances in organic thermoelectric materials: principle mechanisms and emerging carbon-based green energy materials. Polymers 2019;11:167. https://doi.org/10.3390/polym11010167.
[119] Diao Y, Shaw L, Bao Z, Mannsfeld SCB. Morphology control strategies for solution-processed organic semiconductor thin films. Energy Environ Sci 2014;7:2145–59. https://doi.org/10.1039/C4EE00688G.
[120] Wei Q, Mukaida M, Kirihara K, Naitoh Y, Ishida T. Recent progress on PEDOT-based thermoelectric materials. Materials 2015;8:732–50. https://doi.org/10.3390/ma8020732.
[121] Yvenou E, Sandroni M, Carella A, Gueye MN, Faure-Vincent J, Pouget S, et al. Spray-coated PEDOT:OTf films: thermoelectric properties and integration into a printed thermoelectric generator. Mater Chem Front 2020;4:2054–63. https://doi.org/10.1039/D0QM00265H.
[122] Elmoughni HM, Menon AK, Wolfe RMW, Yee SK. A textile-integrated polymer thermoelectric generator for body heat harvesting. Adv. Mater. Technol. 2019;4:1800708. https://doi.org/10.1002/admt.201800708.
[123] Mytafides CK, Tzounis L, Karalis G, Formanek P, Paipetis AS. High-power all-carbon fully printed and wearable SWCNT-based organic thermoelectric generator. ACS Appl Mater Interfaces 2021;13:11151–65. https://doi.org/10.1021/acsami.1c00414.
[124] Culebras M, Uriol B, Gómez CM, Cantarero A. Controlling the thermoelectric properties of polymers: application to PEDOT and polypyrrole. Phys Chem Chem Phys 2015;17:15140–5. https://doi.org/10.1039/C5CP01940K.
[125] Wu J, Sun Y, Pei W-B, Huang L, Xu W, Zhang Q. Polypyrrole nanotube film for flexible thermoelectric application. Synth Met 2014;196:173–7. https://doi.org/10.1016/j.synthmet.2014.08.001.
[126] Wang J, Cai K, Shen S, Yin J. Preparation and thermoelectric properties of multi-walled carbon nanotubes/polypyrrole composites. Synth Met 2014;195:132–6. https://doi.org/10.1016/j.synthmet.2014.06.003.
[127] Yao Q, Chen L, Zhang W, Liufu S, Chen X. Enhanced thermoelectric performance of single-walled carbon nanotubes/polyaniline hybrid nanocomposites. ACS Nano 2010;4:2445–51. https://doi.org/10.1021/nn1002562.
[128] Zhang K, Davis M, Qiu J, Hope-Weeks L, Wang S. Thermoelectric properties of porous multi-walled carbon nanotube/polyaniline core/shell nanocomposites. Nanotechnology 2012;23:385701. https://doi.org/10.1088/0957-4484/23/38/385701.
[129] Zhao Y, Tang G-S, Yu Z-Z, Qi J-S. The effect of graphite oxide on the thermoelectric properties of polyaniline. Carbon N Y 2012;50:3064–73. https://doi.org/10.1016/j.carbon.2012.03.001.
[130] Cowen LM, Atoyo J, Carnie MJ, Baran D, Schroeder BC. Review—organic materials for thermoelectric energy generation. ECS Journal of Solid State Science and Technology 2017;6:N3080–8. https://doi.org/10.1149/2.0121703jss.
[131] Singh RK, Kumar J, Singh R, Kant R, Chand S, Kumar V. Micromorphology, photophysical and electrical properties of pristine and ferric chloride doped poly (3-hexylthiophene) films. Mater Chem Phys 2007;104:390–6. https://doi.org/10.1016/j.matchemphys.2007.01.024.
[132] Zhang Q, Sun Y, Xu W, Zhu D. Thermoelectric energy from flexible P3HT films doped with a ferric salt of triflimide anions. Energy Environ Sci 2012;5:9639. https://doi.org/10.1039/c2ee23006b.
[133] Xuan Y, Liu X, Desbief S, Leclère P, Fahlman M, Lazzaroni R, et al. Thermoelectric properties of conducting polymers: the case of poly(3-hexylthiophene). Phys Rev B 2010;82:115454. https://doi.org/10.1103/PhysRevB.82.115454.
[134] Lee W, Hong CT, Kwon OH, Yoo Y, Kang YH, Lee JY, et al. Enhanced thermoelectric performance of bar-coated SWCNT/P3HT thin films. ACS Appl Mater Interfaces 2015;7:6550–6. https://doi.org/10.1021/acsami.5b00626.
[135] Raja V, Hu Z, Chen G. Progress in poly(2,5-bis(3-alkylthiophen-2-yl)thieno[3,2-b] thiophene) composites for thermoelectric application. Compos Commun 2021;27:100886. https://doi.org/10.1016/j.coco.2021.100886.
[136] Venkateshvaran D, Kronemeijer AJ, Moriarty J, Emin D, Sirringhaus H. Field-effect modulated Seebeck coefficient measurements in an organic polymer using a microfabricated on-chip architecture. Apl Mater 2014;2:032102. https://doi.org/10.1063/1.4867224.
[137] Cowen LM, Atoyo J, Carnie MJ, Baran D, Schroeder BC. Review—organic materials for thermoelectric energy generation. ECS Journal of Solid State Science and Technology 2017;6:N3080–8. https://doi.org/10.1149/2.0121703jss.
[138] Jones BA, Ahrens MJ, Yoon M-H, Facchetti A, Marks TJ, Wasielewski MR. High-mobility air-stable n-type semiconductors with processing versatility: dicyanoperylene-3,4:9,10-bis(dicarboximides). Angew Chem Int Ed 2004;43:6363–6. https://doi.org/10.1002/anie.200461324.
[139] Tonga M. A rational ternary design of P3HT/insulating polymers–CNTs/P3HT for the enhanced thermoelectric performances. Compos Interfac 2022;29:197–213. https://doi.org/10.1080/09276440.2021.1913900.
[140] Wang S, Zhou Y, Liu Y, Wang L, Gao C. Enhanced thermoelectric properties of polyaniline/polypyrrole/carbon nanotube ternary composites by treatment with a secondary dopant using ferric chloride. J Mater Chem C Mater 2020;8:528–35. https://doi.org/10.1039/C9TC06300E.
[141] Cho C, Wallace KL, Tzeng P, Hsu J-H, Yu C, Grunlan JC. Outstanding low temperature thermoelectric power factor from completely organic thin films enabled by multidimensional conjugated nanomaterials. Adv Energy Mater 2016;6:1502168. https://doi.org/10.1002/aenm.201502168.
[142] Zhou J, Peng P, Li Z, Liang L, Huang X, Lv H, et al. Interfacial architecting with anion treatment for enhanced thermoelectric power of flexible ternary polymer nanocomposites. J Mater Chem A Mater 2021;9:20544–52. https://doi.org/10.1039/D1TA04698E.
[143] Jones BA, Facchetti A, Wasielewski MR, Marks TJ. Tuning orbital energetics in arylene diimide semiconductors. Materials design for ambient stability of n-type charge transport. J Am Chem Soc 2007;129:15259–78. https://doi.org/10.1021/ja075242e.
[144] Sun Y, Di C, Xu W, Zhu D. Advances in n-type organic thermoelectric materials and devices. Adv Electron Mater 2019;5:1800825. https://doi.org/10.1002/aelm.201800825.
[145] Zuo G, Li Z, Wang E, Kemerink M. High seebeck coefficient and power factor in n-type organic thermoelectrics. Adv Electron Mater 2018;4:1700501. https://doi.org/10.1002/aelm.201700501.
[146] Liu J, Qiu L, Alessandri R, Qiu X, Portale G, Dong J, et al. Enhancing molecular n-type doping of donor-acceptor copolymers by tailoring side chains. Adv Mater 2018;30:1704630. https://doi.org/10.1002/adma.201704630.
[147] Liu J, van der Zee B, Alessandri R, Sami S, Dong J, Nugraha MI, et al. N-type organic thermoelectrics: demonstration of ZT > 0.3. Nat Commun 2020;11:5694. https://doi.org/10.1038/s41467-020-19537-8.
[148] Orrill M, LeBlanc S. Printed thermoelectric materials and devices: fabrication techniques, advantages, and challenges. J Appl Polym Sci 2017;134. https://doi.org/10.1002/app.44256.

[149] Bubnova O, Khan ZU, Malti A, Braun S, Fahlman M, Berggren M, et al. Optimization of the thermoelectric figure of merit in the conducting polymer poly (3,4-ethylenedioxythiophene). Nat Mater 2011;10:429–33. https://doi.org/10.1038/nmat3012.
[150] Hong CT, Kang YH, Ryu J, Cho SY, Jang K-S. Spray-printed CNT/P3HT organic thermoelectric films and power generators. J Mater Chem A Mater 2015;3:21428–33. https://doi.org/10.1039/C5TA06096F.
[151] Yang C-Y, Stoeckel M-A, Ruoko T-P, Wu H-Y, Liu X, Kolhe NB, et al. A high-conductivity n-type polymeric ink for printed electronics. Nat Commun 2021;12:2354. https://doi.org/10.1038/s41467-021-22528-y.
[152] Wei Q, Mukaida M, Kirihara K, Naitoh Y, Ishida T. Polymer thermoelectric modules screen-printed on paper. RSC Adv 2014;4:28802–6. https://doi.org/10.1039/C4RA04946B.
[153] Søndergaard RR, Hösel M, Espinosa N, Jørgensen M, Krebs FC. Practical evaluation of organic polymer thermoelectrics by large-area R2R processing on flexible substrates. Energy Sci Eng 2013;1:81–8. https://doi.org/10.1002/ese3.8.
[154] We JH, Kim SJ, Cho BJ. Hybrid composite of screen-printed inorganic thermoelectric film and organic conducting polymer for flexible thermoelectric power generator. Energy 2014;73:506–12. https://doi.org/10.1016/j.energy.2014.06.047.
[155] Kee S, Haque MA, Corzo D, Alshareef HN, Baran D. Self-healing and stretchable 3D-printed organic thermoelectrics. Adv Funct Mater 2019;29:1905426. https://doi.org/10.1002/adfm.201905426.
[156] Gopinath KP, Vo D-VN, Gnana Prakash D, Adithya Joseph A, Viswanathan S, Arun J. Environmental applications of carbon-based materials: a review. Environ Chem Lett 2021;19:557–82. https://doi.org/10.1007/s10311-020-01084-9.
[157] Ma X, Zhi D, Jiang Z, He Z, Sun Y, Zhang F. Hybrid/composite organic thermoelectric materials. Organic Thermoelectrics 2022:123–59. https://doi.org/10.1002/9783527835492.ch5. Wiley.
[158] Claussen JC, Shi J, Rout CS, Artiles MS, Roushar MM, Stensberg MC, et al. Nano-sized biosensors for medical applications. Biosensors for Medical Applications 2012:65–102. https://doi.org/10.1533/9780857097187.1.65. Elsevier.
[159] Rogl G, Zehetbauer MJ, Rogl PF. The effect of severe plastic deformation on thermoelectric performance of skutterudites, half-heuslers and Bi-tellurides. Mater Trans 2019;60:2071–85. https://doi.org/10.2320/matertrans.MF201941.
[160] Yu C, Choi K, Yin L, Grunlan JC. Light-weight flexible carbon nanotube based organic composites with large thermoelectric power factors. ACS Nano 2011;5:7885–92. https://doi.org/10.1021/nn202868a.
[161] Najmi L, Hu Z. Review on molecular dynamics simulations of effects of carbon nanotubes (CNTs) on electrical and thermal conductivities of CNT-modified polymeric composites. J Composites Sci 2023;7:165. https://doi.org/10.3390/jcs7040165.
[162] Wei J, Wu D, Liu C, Zhong F, Cao G, Li B, et al. Free-standing p-Type SWCNT/MXene composite films with low thermal conductivity and enhanced thermoelectric performance. Chem Eng J 2022;439:135706. https://doi.org/10.1016/j.cej.2022.135706.
[163] Bradley K, Jhi S-H, Collins PG, Hone J, Cohen ML, Louie SG, et al. Is the intrinsic thermoelectric power of carbon nanotubes positive? Phys Rev Lett 2000;85:4361–4. https://doi.org/10.1103/PhysRevLett.85.4361.
[164] Nonoguchi Y, Nakano M, Murayama T, Hagino H, Hama S, Miyazaki K, et al. Simple salt-coordinated n-type nanocarbon materials stable in air. Adv Funct Mater 2016;26:3021–8. https://doi.org/10.1002/adfm.201600179.
[165] Yao Q, Wang Q, Wang L, Chen L. Abnormally enhanced thermoelectric transport properties of SWNT/PANI hybrid films by the strengthened PANI molecular ordering. Energy Environ Sci 2014;7:3801–7. https://doi.org/10.1039/C4EE01905A.
[166] Zhang Q, Wang W, Li J, Zhu J, Wang L, Zhu M, et al. Preparation and thermoelectric properties of multi-walled carbon nanotube/polyaniline hybrid nanocomposites. J Mater Chem A Mater 2013;1:12109. https://doi.org/10.1039/c3ta12353g.
[167] Hong CT, Lee W, Kang YH, Yoo Y, Ryu J, Cho SY, et al. Effective doping by spin-coating and enhanced thermoelectric power factors in SWCNT/P3HT hybrid films. J Mater Chem A Mater ;3:12314–9. https://doi.org/10.1039/C5TA02443A.
[168] Wang L, Jia X, Wang D, Zhu G, Li J. Preparation and thermoelectric properties of polythiophene/multiwalled carbon nanotube composites. Synth Met 2013;181:79–85. https://doi.org/10.1016/j.synthmet.2013.08.011.
[169] Moriarty GP, De S, King PJ, Khan U, Via M, King JA, et al. Thermoelectric behavior of organic thin film nanocomposites. J Polym Sci B Polym Phys 2013;51:119–23. https://doi.org/10.1002/polb.23186.
[170] Wang J, Cai K, Shen S, Yin J. Preparation and thermoelectric properties of multi-walled carbon nanotubes/polypyrrole composites. Synth Met 2014;195:132–6. https://doi.org/10.1016/j.synthmet.2014.06.003.
[171] Wang L, Jia X, Wang D, Zhu G, Li J. Preparation and thermoelectric properties of polythiophene/multiwalled carbon nanotube composites. Synth Met 2013;181:79–85. https://doi.org/10.1016/j.synthmet.2013.08.011.
[172] Geim AK, Novoselov KS. The rise of graphene. Nat Mater 2007;6:183–91. https://doi.org/10.1038/nmat1849.
[173] Hicks LD, Dresselhaus MS. Thermoelectric figure of merit of a one-dimensional conductor. Phys Rev B 1993;47:16631–4. https://doi.org/10.1103/PhysRevB.47.16631.
[174] Pan C, Zhang L, Pan Z, Chen M, Liu Y, Huang G, et al. A simple strategy to fabricate polyaniline/expanded graphite composites with improved power factor. Mater Chem Phys 2015;167:315–9. https://doi.org/10.1016/j.matchemphys.2015.10.050.
[175] Li F, Cai K, Shen S, Chen S. Preparation and thermoelectric properties of reduced graphene oxide/PEDOT:PSS composite films. Synth Met 2014;197:58–61. https://doi.org/10.1016/j.synthmet.2014.08.014.
[176] Yoo D, Kim J, Kim JH. Direct synthesis of highly conductive poly(3,4-ethylenedioxythiophene):poly(4-styrenesulfonate) (PEDOT:PSS)/graphene composites and their applications in energy harvesting systems. Nano Res 2014;7:717–30. https://doi.org/10.1007/s12274-014-0433-z.
[177] Ube T, Koyanagi J, Kosaki T, Fujimoto K, Yokozeki T, Ishiguro T, et al. Fabrication of well-isolated graphene and evaluation of thermoelectric performance of polyaniline–graphene composite film. J Mater Sci 2019;54:3904–13. https://doi.org/10.1007/s10853-018-3129-z.
[178] Zhang K, Wang S, Zhang X, Zhang Y, Cui Y, Qiu J. Thermoelectric performance of p-type nanohybrids filled polymer composites. Nano Energy 2015;13:327–35. https://doi.org/10.1016/j.nanoen.2015.03.004.
[179] Hsieh Y-Y, Zhang Y, Zhang L, Fang Y, Kanakaraaj SN, Bahk J-H, et al. High thermoelectric power-factor composites based on flexible three-dimensional graphene and polyaniline. Nanoscale 2019;11:6552–60. https://doi.org/10.1039/C8NR10537E.
[180] Wang L, Yao Q, Bi H, Huang F, Wang Q, Chen L. PANI/graphene nanocomposite films with high thermoelectric properties by enhanced molecular ordering. J Mater Chem A Mater 2015;3:7086–92. https://doi.org/10.1039/C4TA06422D.
[181] Xu K, Chen G, Qiu D. Convenient construction of poly(3,4-ethylenedioxythiophene)–graphene pie-like structure with enhanced thermoelectric performance. J Mater Chem A Mater 2013;1:12395. https://doi.org/10.1039/c3ta12691a.
[182] Lu Y, Song Y, Wang F. Thermoelectric properties of graphene nanosheets-modified polyaniline hybrid nanocomposites by an in situ chemical polymerization. Mater Chem Phys 2013;138:238–44. https://doi.org/10.1016/j.matchemphys.2012.11.052.
[183] Liang L, Fan J, Wang M, Chen G, Sun G. Ternary thermoelectric composites of polypyrrole/PEDOT:PSS/carbon nanotube with unique layered structure prepared by one-dimensional polymer nanostructure as template. Compos Sci Technol 2020;187:107948. https://doi.org/10.1016/j.compscitech.2019.107948.
[184] Cho C, Culebras M, Wallace KL, Song Y, Holder K, Hsu J-H, et al. Stable n-type thermoelectric multilayer thin films with high power factor from carbonaceous nanofillers. Nano Energy 2016;28:426–32. https://doi.org/10.1016/j.nanoen.2016.08.063.
[185] Cho C, Wallace KL, Tzeng P, Hsu J-H, Yu C, Grunlan JC. Outstanding low temperature thermoelectric power factor from completely organic thin films enabled by multidimensional conjugated nanomaterials. Adv Energy Mater 2016;6:1502168. https://doi.org/10.1002/aenm.201502168.
[186] Li G, Hu Y, Chen J, Liang L, Liu Z, Fu J, et al. Thermoelectric and photoelectric dual modulated sensors for human Internet of Things application in accurate fire recognition and warning. Adv Funct Mater 2023. https://doi.org/10.1002/adfm.202303861.
[187] Bae EJ, Kang YH, Lee C, Cho SY. Engineered nanocarbon mixing for enhancing the thermoelectric properties of a telluride-PEDOT:PSS nanocomposite. J Mater Chem A Mater 2017;5:17867–73. https://doi.org/10.1039/C7TA04280A.
[188] Xiang J, Drzal LT. Templated growth of polyaniline on exfoliated graphene nanoplatelets (GNP) and its thermoelectric properties. Polymer 2012;53:4202–10. https://doi.org/10.1016/j.polymer.2012.07.029.
[189] Bandaru S, Jastrzębska AM, Birowska M. Recent progress in thermoelectric MXene-based structures versus other 2D materials. Appl Mater Today 2023;34:101902. https://doi.org/10.1016/j.apmt.2023.101902.
[190] Zhu M, Lu C, Liu L. Progress and challenges of emerging MXene based materials for thermoelectric applications. iScience 2023;26:106718. https://doi.org/10.1016/j.isci.2023.106718.
[191] Wang Y, Bai Z, Guo Y, Liu C, Jiang Q, Jiang F, et al. Recent advances in 2D material/conducting polymer composites for thermoelectric energy conversion. Macromol Mater Eng 2022;307. https://doi.org/10.1002/mame.202200107.
[192] Deng L, Liu Y, Zhang Y, Wang S, Gao P. Organic thermoelectric materials: niche harvester of thermal energy. Adv Funct Mater 2023;33. https://doi.org/10.1002/adfm.202210770.
[193] Qian Y, Zhou P, Wang Y, Zheng Y, Luo Z, Chen L. A PEDOT:PSS/MXene-based actuator with self-powered sensing function by incorporating a photo-thermoelectric generator. RSC Adv 2023;13:32722–33. https://doi.org/10.1039/D3RA06290B.
[194] Jiang C, Chen J, Lai X, Li H, Zeng X, Zhao Y, et al. Mechanically robust and multifunctional polyimide/MXene composite aerogel for smart fire protection. Chem Eng J 2022;434:134630. https://doi.org/10.1016/j.cej.2022.134630.
[195] Ding W, Liu P, Bai Z, Wang Y, Liu G, Jiang Q, et al. Constructing layered MXene/CNTs composite film with 2D–3D sandwich structure for high thermoelectric performance. Adv Mater Interfac 2020;7. https://doi.org/10.1002/admi.202001340.
[196] Jin X, Yang Z, Huang C, Yang J, Wang Y. PEDOT:PSS/MXene/PEG composites with remarkable thermal management performance and excellent HF-band & X-band electromagnetic interference shielding efficiency for electronic packaging. Chem Eng J 2022;448:137599. https://doi.org/10.1016/j.cej.2022.137599.
[197] Faruk O, Adak B. Recent advances in PEDOT:PSS integrated graphene and MXene-based composites for electrochemical supercapacitor applications. Synth Met 2023;297:117384. https://doi.org/10.1016/j.synthmet.2023.117384.
[198] Wustoni S, Saleh A, El-Demellawi JK, Koklu A, Hama A, Druet V, et al. MXene improves the stability and electrochemical performance of electropolymerized PEDOT films. Apl Mater 2020;8. https://doi.org/10.1063/5.0023187.

[199] Guan X, Feng W, Wang X, Venkatesh R, Ouyang J. Significant enhancement in the seebeck coefficient and power factor of p-type poly(3,4-ethylenedioxythiophene): poly(styrenesulfonate) through the incorporation of n-type MXene. ACS Appl Mater Interfaces 2020;12:13013–20. https://doi.org/10.1021/acsami.9b21185.
[200] Jung KK, Jung Y, Choi CJ, Lee JM, Ko JS. Flexible thermoelectric generator with polydimethyl siloxane in thermoelectric material and substrate. Curr Appl Phys 2016;16:1442–8. https://doi.org/10.1016/j.cap.2016.08.010.
[201] Bell LE. Cooling, heating, generating power, and recovering waste heat with thermoelectric systems. Science 2008;321:1457–61. https://doi.org/10.1126/science.1158899.
[202] Shakouri A. Recent developments in semiconductor thermoelectric physics and materials. Annu Rev Mater Res 2011;41:399–431. https://doi.org/10.1146/annurev-matsci-062910-100445.
[203] Sootsman JR, Chung DY, Kanatzidis MG. New and old concepts in thermoelectric materials. Angew Chem Int Ed 2009;48:8616–39. https://doi.org/10.1002/anie.200900598.
[204] Hamid Elsheikh M, Shnawah DA, Sabri MFM, Said SBM, Haji Hassan M, Ali Bashir MB, et al. A review on thermoelectric renewable energy: principle parameters that affect their performance. Renew Sustain Energy Rev 2014;30:337–55. https://doi.org/10.1016/j.rser.2013.10.027.
[205] Riffat SB, Ma X. Thermoelectrics: a review of present and potential applications. Appl Therm Eng 2003;23:913–35. https://doi.org/10.1016/S1359-4311(03)00012-7.
[206] Haghi M, Thurow K, Stoll R. Wearable devices in medical Internet of Things: scientific research and commercially available devices. Healthc Inform Res 2017;23:4. https://doi.org/10.4258/hir.2017.23.1.4.
[207] Cohen ML. Measurement of the thermal properties of human SKIN. A review. J Invest Dermatol 1977;69:333–8. https://doi.org/10.1111/1523-1747.ep12507965.
[208] Hossain M. Frugal innovation: a systematic literature review. SSRN Electron J 2016. https://doi.org/10.2139/ssrn.2768254.
[209] Armand Ngouateu Wouagfack P, Tenkeng M, Lissouck D, Tchinda R. A review on exergy analysis of solar refrigeration technologies. Ind Eng 2020;4:14. https://doi.org/10.11648/j.ie.20200402.11.
[210] Piggott A. Detailed transient multiphysics model for fast and accurate design, simulation and optimization of a thermoelectric generator (TEG) or thermal energy harvesting device. J Electron Mater 2019;48:5442–52. https://doi.org/10.1007/s11664-019-06952-x.
[211] Pourkiaei SM, Ahmadi MH, Sadeghzadeh M, Moosavi S, Pourfayaz F, Chen L, et al. Thermoelectric cooler and thermoelectric generator devices: a review of present and potential applications, modeling and materials. Energy 2019;186:115849. https://doi.org/10.1016/j.energy.2019.07.179.
[212] Zheng C, Xiang L, Jin W, Shen H, Zhao W, Zhang F, et al. A flexible self-powered sensing element with integrated organic thermoelectric generator. Adv Mater Technol 2019;4. https://doi.org/10.1002/admt.201900247.
[213] Jung M, Jeon S, Bae J. Scalable and facile synthesis of stretchable thermoelectric fabric for wearable self-powered temperature sensors. RSC Adv 2018;8:39992–9. https://doi.org/10.1039/C8RA06664G.
[214] Hong SY, Oh JH, Park H, Yun JY, Jin SW, Sun L, et al. Polyurethane foam coated with a multi-walled carbon nanotube/polyaniline nanocomposite for a skin-like stretchable array of multi-functional sensors. NPG Asia Mater 2017;9:e448. https://doi.org/10.1038/am.2017.194. e448.
[215] Yang Y, Lin Z-H, Hou T, Zhang F, Wang ZL. Nanowire-composite based flexible thermoelectric nanogenerators and self-powered temperature sensors. Nano Res 2012;5:888–95. https://doi.org/10.1007/s12274-012-0272-8.
[216] Jung M, Jeon S, Bae J. Scalable and facile synthesis of stretchable thermoelectric fabric for wearable self-powered temperature sensors. RSC Adv 2018;8:39992–9. https://doi.org/10.1039/C8RA06664G.
[217] Wang Y-F, Sekine T, Takeda Y, Yokosawa K, Matsui H, Kumaki D, et al. Fully printed PEDOT:PSS-based temperature sensor with high humidity stability for wireless healthcare monitoring. Sci Rep 2020;10:2467. https://doi.org/10.1038/s41598-020-59432-2.